REPORT DOCUMENTATION PAGE

AFRL-SR-BL-TR-98-

0197

Public reporting burden for this collection of information is estimated to average 1 hour per response, including the time the data needed, and completing and reviewing this collection of information. Send comments regarding this burden es reducing this burden to Washington Headquarters Services, Directorate for Information Operations and Reports, 1215 Management and Budget, Paperwork Reduction Project (0704-0188), Washington, DC 20503

nd maintaining
ggestions for
> the Office of

1. AGENCY USE ONLY (Leave blank)	2. REPORT DATE 11 Feb 1998	3. REPORT TYPE AND DATES COVERED Final: 1 Sept 1996 – 31 Aug 1997

4. TITLE AND SUBTITLE	5. FUNDING NUMBERS
High Performance Electrooptic Polymers and Excited State Enhancements	Grant F-49620-94-1-0252 2303/CS 61102F

6. AUTHOR(S)
Garito, Anthony F.

7. PERFORMING ORGANIZATION NAME(S) AND ADDRESS(ES)	8. PERFORMING ORGANIZATION REPORT NUMBER
University of Pennsylvania Physics & Astronomy 209 South 33rd Street Philadelphia, PA 19104-6396	F-AFG-520475

9. SPONSORING / MONITORING AGENCY NAME(S) AND ADDRESS(ES)	10. SPONSORING / MONITORING AGENCY REPORT NUMBER
AFOSR/NL 110 Duncan Avenue Room B115 Bolling AFB, DC 20332-8080	

11. SUPPLEMENTARY NOTES

12a. DISTRIBUTION / AVAILABILITY STATEMENT

Approved for public release;
distribution is unlimited.

DISTRIBUTION STATEMENT A
Approved for public release;
Distribution Unlimited

12b. DISTRIBUTION CODE

13. ABSTRACT (Maximum 200 Words)
The enhancement of the third order nonlinear optical susceptibility X^3 in the conjugated linear chain has been studied both theoretically and experimentally, when the system is optically pumped to electronic excited states. Enhancements as high as 1000 times have been achieved.

19980223 131

14. SUBJECT TERMS			15. NUMBER OF PAGES 56
nonlinear optics, third order, excited state, Degenerate four wave mixing (DFWM)			16. PRICE CODE

17. SECURITY CLASSIFICATION OF REPORT Unclassified	18. SECURITY CLASSIFICATION OF THIS PAGE Unclassified	19. SECURITY CLASSIFICATION OF ABSTRACT Unclassified	20. LIMITATION OF ABSTRACT UL

NSN 7540-01-280-5500

Standard Form 298 (Rev. 2-89)
Prescribed by ANSI Std. Z39-18
298-102

DTIC QUALITY INSPECTED 3

FINAL REPORT

September 1, 1996 through August 31, 1997

HIGH PERFORMANCE ELECTROOPTIC POLYMERS
AND
EXCITED STATE ENHANCEMENTS

PRINCIPAL INVESTOR: Professor Anthony F. Garito   (215)898-5810

PROGRAM MANAGER: Dr. Charles Lee   (202)767-4960

University of Pennsylvania
209 South 33rd Street
Philadelphia, PA 19104

1.0 Status of Effort

Our objective is to understand the dynamics of the excited state enhancement of the third order nonlinear optical susceptibility by studying the time evolution of the excited state enhanced nonresonant degenerate four wave mixing (DFWM) in the forward phase conjugate geometry [62,63]. In this technique (see Figure 1.1), two probe beams of comparable intensities are focused onto the sample contained in a cell of length L. The intersecting angle is small, $\theta < \sqrt{\dfrac{\lambda}{L}}$. The interference pattern of two probe beams forms an intensity grating that modulates the nonlinear index of refraction of the sample material to create an index of refraction grating through the intensity dependent index of refraction mechanism. This index of refraction grating then diffracts the probe beam into a new direction. In terms of the wave vectors shown in Figure 1.1, the new directions of the
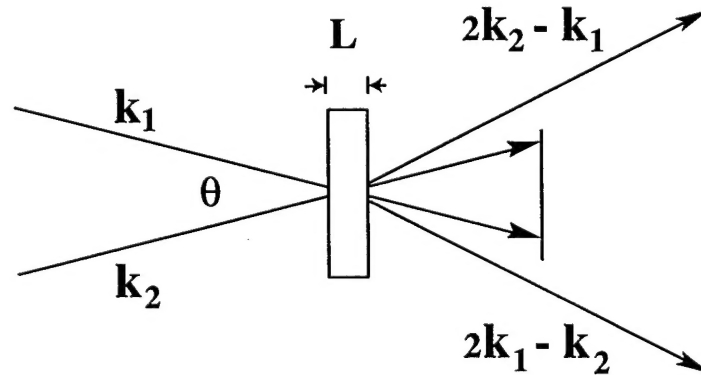

Figure 1.1 DFWM experiment. DFWM is performed by overlapping two probe beams, $\mathbf{k}_1$ and $\mathbf{k}_2$, at a small angle $\theta < \sqrt{\dfrac{\lambda}{L}}$. The nonresonant DFWM signals occur in the $2\mathbf{k}_2\text{-}\mathbf{k}_1$ and $2\mathbf{k}_1\text{-}\mathbf{k}_2$ directions.

scattered probe beams, which is the direction of the DFWM signal, can be either $2\mathbf{k}_2\text{-}\mathbf{k}_1$ or $2\mathbf{k}_1\text{-}\mathbf{k}_2$, where $\mathbf{k}_1$ and $\mathbf{k}_2$ are the wave vectors of the two probe beams. As indicated in equation 3.7, the DFWM signal intensity is proportional to the square of $\chi_{ijkl}^{(3)}(-\omega;\omega,\omega,-\omega)$. The polarizations of the $\mathbf{k}_1$ and $\mathbf{k}_2$ probe beams are chosen to be orthogonal in order to eliminate thermal gratings that can contribute to the DFWM signal. The unique feature of this experiment is that, instead of probing for the DFWM signal from the sample in the ground state, the sample is optically pumped to its electronic excited state (see Figure 1.2). The temporal response of the sample is then investigated by varying the time delay between pumping and probing. When the probing time is very close to the pumping time, half of the molecules are in their excited state according to the two level model, and the two probe beams encounter a mixture of ground state and excited state population, consequently, the measured $\chi_{ijkl}^{(3)}(-\omega;\omega,\omega,-\omega)$ comes from both ground and excited state contributions [18]. For longer probe delay time, the probe encounters a smaller number of excited state molecules, and thus, the measured $\chi_{ijkl}^{(3)}(-\omega;\omega,\omega,-\omega)$ is reduced because the third order nonlinear optical molecular susceptibility of the excited state $\gamma_{ijkl}^{S_2}(-\omega;\omega,\omega,-\omega)$ is orders of magnitude larger than the ground state $\gamma_{ijkl}^{S_0}(-\omega;\omega,\omega,-\omega)$ [8,18]. The probe delay time can be continuously varied from -0.5 ns to 6 ns in order to study the decay of the DFWM signal as a function of time. Since the decay time of the excited state is critically dependent on the energy gap ΔE between the two excited states of DPH [50], varying this energy gap should give us more information about the dynamics of the excited state enhanced $\chi_{ijkl}^{(3)}(-\omega;\omega,\omega,-\omega)$.
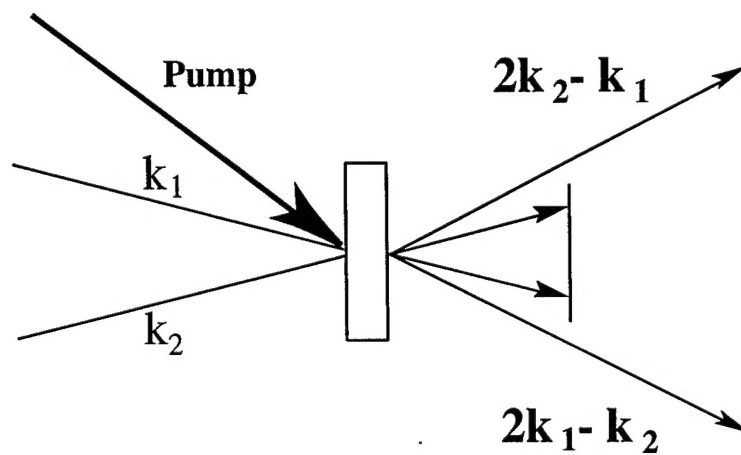
Figure 1.2 Excited state DFWM experiment. Excited state degenerate four wave mixing is carried out by bringing a resonant pump into the sample and overlapping it with the nonresonant probes to generate the excited state DFWM signal.

Fluorescence and absorption studies of DPH solutions indicate that the ΔE can be varied effectively by changing the solvents used in the solutions. Several solvents are used in this study for a wide range of energy gaps.

2.0   Accomplishment

2.1 Degnerated Four Wave Mixing (DFWM)

The forward DFWM is shown in Figure 1.3. The 30 ps, 1064 nm output from a Nd:YAG laser is split into 2 probe beams. They are then focused in coincidence on the sample at a small angle, θ. The DFWM signal in the $2\mathbf{k}_2$-$\mathbf{k}_1$ direction is detected by a PMT. By symmetry, there is also a signal in the $2\mathbf{k}_1$-$\mathbf{k}_2$ direction. The intersecting angle where the two probe beams cross in this experiment, is determined by the sample length and the probing wavelength in equation 2.5. A sample cell with a thickness of 0.5 mm is used. Thicker and thinner cells were tried but the 0.5 mm cell works best for this study. The thicker cell requires a smaller angle in order to get close to perfect phase matching. But the smaller angle makes isolation of the signal very difficult. The problem with the thinner cell is scattering from the cell itself. When the very strong probe beams focus inside the cell, parts of them are scattered by the cell and result in an increase in the background scattering. The other factor that is considered when choosing the cell is the interaction region. Figure 1.4 compares the interaction regions for small and large angles, θ. It is clear that in order to get a larger interaction region a smaller angle must be
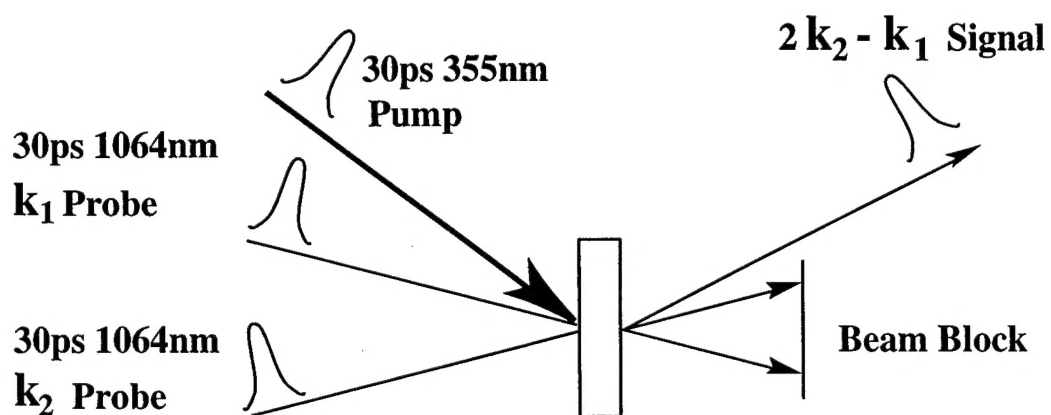
Figure 1.3 Forward excited state DFWM experiment. The two probes are 30 ps, 1064 nm beams from a Nd:YAG laser, focused to overlap on the sample where a 30 ps, 355 nm pump, used to excite the sample molecules to their excited state, is also focused.
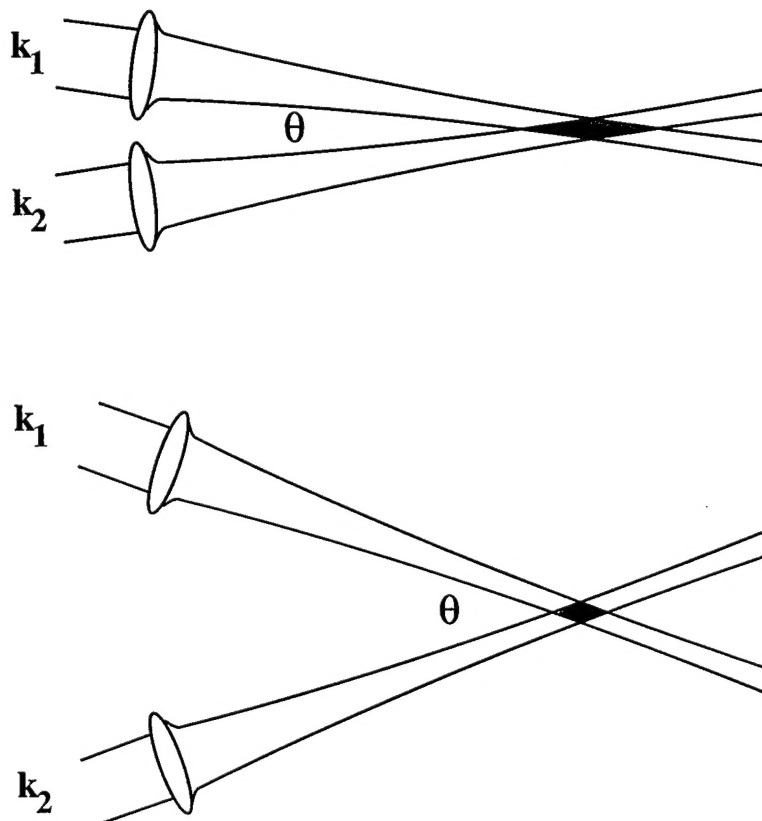
Figure 1.4 Comparison of interaction regions and the intersecting angles, θ. Larger the interaction regions, where the third order nonlinear optical process occurs, can be achieved using a smaller intersecting angles, θ, between the two probe beams.

used. To create the excited state, the sample is pumped by a focused 355 nm beam at the interaction region of the two probe beams. The pump and probes are blocked after they pass through the sample cell, with only the signal detected (Figure 1.3).

2.2 Experimental Layout

The experimental layout is shown in Figure 1.5. Both the 355 nm pump beam and the 1064 nm probe beams are output from a Q-switched, mode-locked Nd:YAG laser. The 1064 nm is the fundamental output wavelength. The 355 nm output is the result of mixing 1064 nm and its second harmonic generation at 532 nm in a BBO crystal. The 355 nm output intensity is around 1 mJ. After passing through long pass filters to eliminate the 355 nm and 532 nm beams, the 1064 nm beam is collimated using a telescope, reducing its diameter to around 4 mm. It is then split into two beams, hereafter called k_1 and k_2 beams according to their direction at the sample cell. These two beams are used as probe beams in the DFWM experiment. The intensities of the two probe beams are approximately equal as a result of splitting the fundamental 1064 nm beam with a beam dielectric splitter coated for 60% reflecting of S-polarized light. Each probe beam travels through a half-wave plate and a prism polarizer that allow selection of the polarization and intensity. For the purpose of this study, k_1 beam is selected to be horizontally polarized with the k_2 beam vertically polarized. The k_1 beam also travels through an adjustable optical delay line so that the path length difference between the two probe beams can be varied. This optical delay line can adjust the delay time between the
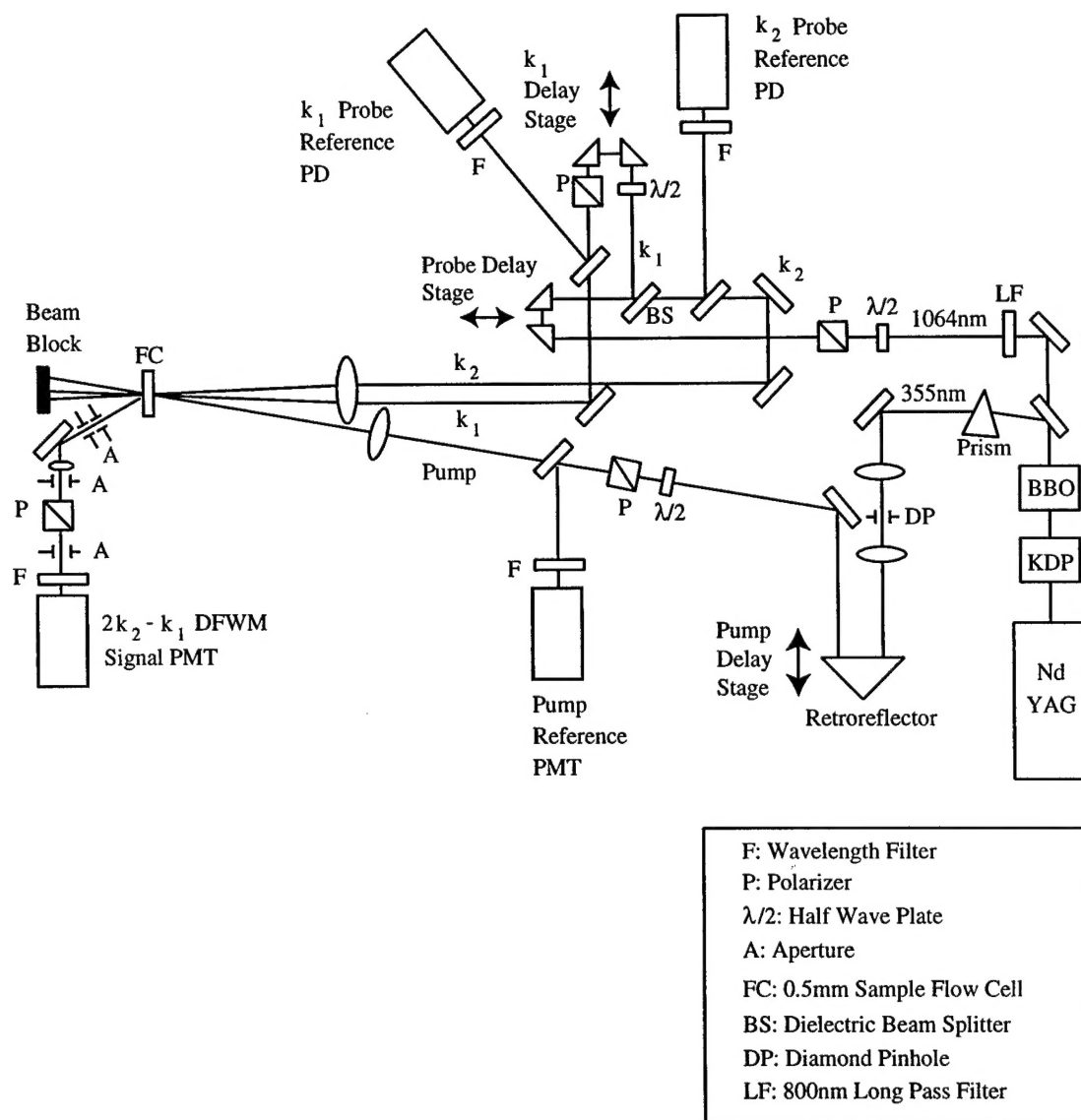
Figure 1.5 Excited state DFWM experimental layout. The pump and probe delay stages allow for dynamical studies of excited state DFWM.

$\mathbf{k}_1$ and $\mathbf{k}_2$ beams, which is the difference in their arrival times at the sample cell, from -100 ps to +100 ps. This is found to be very useful when finding the maximum temporal overlap between the two probe beams, which provides for the highest DFWM signal. After selecting the polarization and adjusting the intensity, both probe beams are aligned to travel parallel to each other, separated by 1 cm. Then single lens focuses them to an intersection point inside the sample cell. The crossing angle is around 2.29 degree and their beam waists are about 100 µm. The intensity of each probe beam entering the sample cell is approximately 0.3 mJ per pulse, which is close to the damage threshold of the fused-silica cell. Any damage to the sample cell in the region where the beams are passing through can cause huge scattering that can overwhelm the DFWM signal.

The 355 nm pump beam is separated from the other laser outputs using a 355 nm high reflector. It also passes through a quartz prism to remove any residues of 532 nm and 1064 nm beams. It is then directed to a half-wave plate and a polarizer for control of polarization and intensity. The 355 nm beam is spatially filtered by focusing it through a diamond pinhole using a lens with a focal length of 45 cm. A smooth pump beam spatial profile is crucial in this experiment. For a smooth beam profile, a small misalignment of the pump beam does not cause a large change in the DFWM signal. In contrast, any hot spots in the pump beam profile can dramatically affect the intensity of the DFWM signal. The lens and a pinhole also form part of a telescope that collimates the pump beam. Beam collimation is very critical to the stability of the pump beam intensity at the sample cell because a diverging (or converging) pump beam would have different beam diameters at the pump lens, and consequently, different beam waists at the sample cell when the path length of the pump beam is changed. After being spatially filtered and collimated, the pump

beam is carefully steered to the retroreflector mounting on the translation stage. This translation stage, driven by a computer controlled stepping motor, is used to vary the delay time between the pump and the two probe beams. The retroreflector reflects the beam back to a pump lens. The pump lens, which is a quartz lens mounted on a two dimensional stage, focuses the pump beam to the probe beams' interaction region on the sample cell. The intensity of the pump beam at the sample cell is around 0.2 mJ.

The sample cell is a 0.5 mm path length fused silica sample flow cell containing the DPH solution. The flow cell is connected to a reservoir of DPH solution. The circulation system is closed and is driven by a micropump. The big reservoir of DPH solution ensures that the concentration of the DPH sample stays constant even if some of the solvent might leak out or vaporize.

The DFWM signal output along the $2\mathbf{k}_2\text{-}\mathbf{k}_1$ direction is isolated from room light and any scattering by a series of apertures and beam blocks. The signal then passes through a polarizer which is used as a polarization analyzer. It is then brought through neutral density filters and a 1064 nm spike filter (interference wavelength filter) into an infrared sensitive PMT. Part of the fundamental 1064 nm is split into a photodiode to be used as a gate signal for data acquisition. All the beams; the $\mathbf{k}_1$ and $\mathbf{k}_2$ probe beams, and the pump beam are also split, using glass slides, into detectors to be used as references.

2.3 Signal Detection

DFWM signals from the PMT (Hamamatsu R3310) are amplified using a current pre-amp [19], and the output is fed into a gate integrator along with an appropriate delay so that it appears in the gate signal window. The gate signal is derived from a photodiode monitoring the output of the laser and its width is set in this experiment to be 100 ns, which is wide enough to cover the entire signal from the PMT. A microcomputer controls the integrator via a CAMAC interface, and accumulates statistics of the DFWM signal on a shot to shot basis. Computer control of the pump half-wave plate, probe arm delay translators, pump arm delay translator, and pump beam lens position allows the computer to quickly carry out measurements of the systematic dependence on pump intensity, relative probe delay, pump-probe delay, and pump-probe overlap, respectively.

Even though the 100 ns wide gate signal window can cut some of the background noise from the detected signal, we still have unavoidable scattering because the detected frequency is the same as the probe frequency. As discussed earlier, the background scattering has been reduced by using a series of apertures, beam blocks, and an analyzer, but if scattering from either the k_1 or the k_2 beam, is also in the $2k_2$-k_1 direction, it will be detected as signal. This is especially true in the forward phase conjugate DFWM where the intersecting angle is very small and the $2k_2$-k_1 direction is very close to the k_2 direction. In addition, both probe beams are not just rays, but diverge from their focal spots on the sample, making the probe beams closer to the direction of the DFWM signal. To eliminate this background scattering, a system of computer controlled shutter is used to block each probe beam, and then to measure and automatically subtract this background scattering from the signal for each data point recorded. A schematic sketch of the shutter system is

shown in Figure 1.6. The computer produces a logic output signal to specify the state of each shutter, whether they block or unblock the beams. The procedure for acquiring data is as follows: (1) measure N shots of the detector intensity, (2) block $\mathbf{k}_1$ probe and subtract the scattering intensity due to N shots of the $\mathbf{k}_2$ probe, (3) block $\mathbf{k}_2$ probe and subtract the scattering intensity due to N shots of $\mathbf{k}_1$ probe. Both of the two probe beams can be blocked at the same time and the measured detector intensity, which is due to the dark current background, can be subtracted from all the detector measurements of DFWM. For the excited state $\chi^{(3)}_{ijkl}(-\omega;\omega,\omega,-\omega)$ measurement, in which the pump beam is involved, another shutter is added for the pump beam and a similar procedure is carried out to eliminate the scattering caused by the pump beam.

Laser drift is another problem that we have to take into account. It occurs because the time used to take each data set is very long due to the low repetition rate, 10 Hz, of the laser. In order to be able to compare data taken at the beginning and the end of the run in which laser drift might occur, the DFWM signals are normalized so that they are independent of the laser intensity. In this experiment, the normalized DFWM signal in the $2\mathbf{k}_2$-$\mathbf{k}_1$ direction is defined by

$$\text{Normalized Signal} = \frac{\langle \text{DFWM Signal} \rangle}{\langle \mathbf{k}_1 \text{ Probe Reference} \rangle \langle \mathbf{k}_2 \text{ Probe Reference} \rangle^2} \qquad (1.1)$$
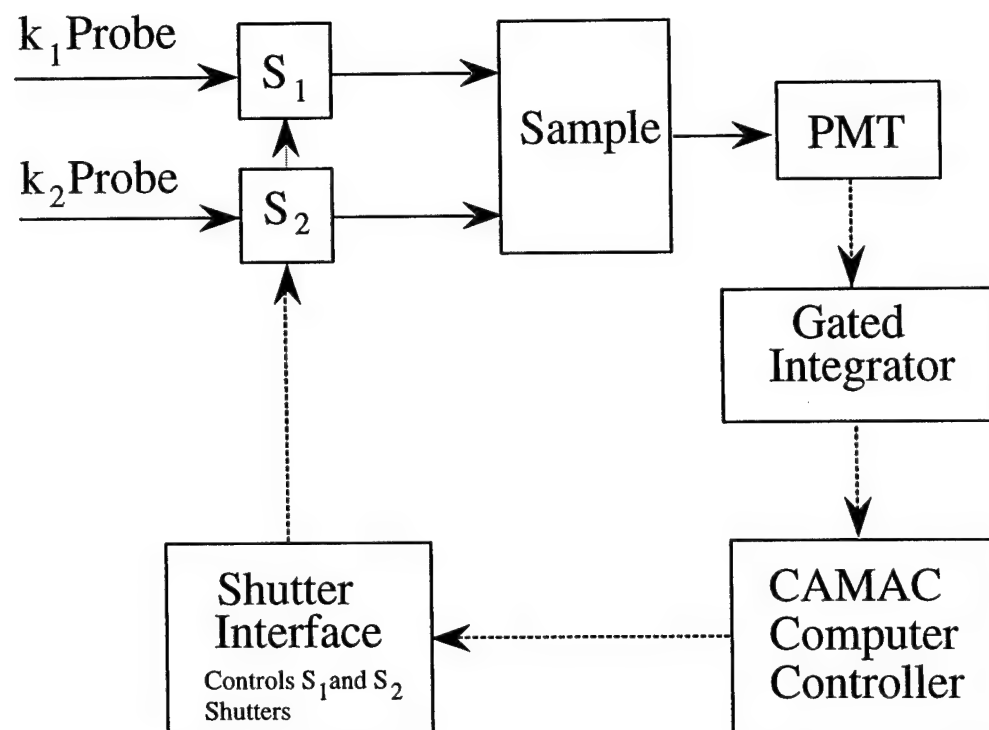
Figure 1.6 Schematic sketch of the shutter control system. The background scattering in the excited state DFWM experiment is reduced by using the computer controlled shutter system. The computer sends out TTL signal to specify the state of each shutter (block/unblock) for each beam in order to measure and then subtract the background scattering from the intensity detected.

where $\langle \ \rangle$ denotes an average over N laser pulses. The quality of the normalization is crucially dependent on the linearity of the response of each detector. For good normalization to be achieved, each detector must have a linear response for the entire range of intensities detected. Any nonlinear response in a detector would cause error in the normalized signal. All detectors used in this study, are found to have linear responses.

3.0 Excited State DFWM

3.1 Polarization Configurations

There are four simple different tensor components of $\chi_{ijkl}^{(3)}(-\omega;\omega,\omega,-\omega)$ that we can study using the setup in DFWM experiment. These different components that produce the DFWM signal are determined by the polarizations of the probe beams. In the $2\mathbf{k}_2\text{-}\mathbf{k}_1$ forward phase conjugate DFWM experiment, the detected polarization follows the polarization of the $\mathbf{k}_1$ probe beam. It can be derived using the following relation between the third order nonlinear polarization and input fields.

$$P_i^{(3)}(2\mathbf{k}_2 - \mathbf{k}_1,\omega) = \chi_{ijkl}^{(3)}(-\omega;\omega,\omega,-\omega)\, E_j(\mathbf{k}_2,\omega)\, E_k(\mathbf{k}_2,\omega)\, E_l^*(\mathbf{k}_1,\omega) \qquad (1.2)$$

where $E_l(\mathbf{k}_1,\omega)$ is the l component (x, y or z) of the $\mathbf{k}_1$ probe electric field. $E_j(\mathbf{k}_2,\omega)$ and $E_k(\mathbf{k}_2,\omega)$ are j and k components (x, y or z) of the $\mathbf{k}_2$ probe electric fields, respectively. $P_i^{(3)}(2\mathbf{k}_2 - \mathbf{k}_1,\omega)$ is the i component (x, y or z) of the third order nonlinear polarization which is the direction of polarization of the output DFWM signal [2]. Because we use two photons from the $\mathbf{k}_2$ probe beam, the polarizations of these two photons are the same; $j = k$. As a result of the symmetry of the third order susceptibility tensor, $\chi_{ijkl}^{(3)}(-\omega;\omega,\omega,-\omega)$ has a nonvanishing value only when $i = l$, that is when the

polarization of the output DFWM signal is the same as the polarization of $\mathbf{k}_1$ probe beam. Therefore, the detector analyzer has to be set to the appropriate polarization, which is the same as the $\mathbf{k}_1$ probe polarization. Using our setup, the experiment can be carried out in four polarization configurations:

Configuration 1: *xxxx* configuration, used to detect $\chi^{(3)}_{xxxx}(-\omega;\omega,\omega,-\omega)$, with both probes and analyzer all horizontally polarized.

Configuration 2: *yyyy* configuration, used to detect $\chi^{(3)}_{yyyy}(-\omega;\omega,\omega,-\omega)$, with both probes and analyzer all vertically polarized.

Configuration 3: *xyyx* configuration, used to detect $\chi^{(3)}_{xyyx}(-\omega;\omega,\omega,-\omega)$, with the $\mathbf{k}_1$ probe horizontally polarized, the $\mathbf{k}_2$ probe vertically polarized and the analyzer horizontally polarized.

Configuration 4: *yxxy* configuration, used to detect $\chi^{(3)}_{yxxy}(-\omega;\omega,\omega,-\omega)$, with the $\mathbf{k}_1$ probe vertically polarized, the $\mathbf{k}_2$ probe horizontally polarized and the analyzer vertically polarized.

The configuration components *ijkl* are the polarizations of the DFWM signal, the two photons from the $\mathbf{k}_2$ probe, and the one photon from the $\mathbf{k}_1$ probe, respectively. Because of the symmetry of $\chi^{(3)}_{ijkl}(-\omega;\omega,\omega,-\omega)$ in an isotropic liquid, $\chi^{(3)}_{xxxx} = \chi^{(3)}_{yyyy}$ and thus we need to observe only the *xxxx* configuration. Similarly, $\chi^{(3)}_{xyyx} = \chi^{(3)}_{yxxy}$ and we need to observe only in the *xyyx* configuration. Equation 1.27 indicates a larger $\chi^{(3)}_{xxxx}(-\omega;\omega,\omega,-\omega)$ compared to $\chi^{(3)}_{xyyx}(-\omega;\omega,\omega,-\omega)$, so the *xxxx* configuration would yield a larger DFWM signal that is easily observed. Unfortunately, there is a large contribution to the DFWM signal from the thermal grating, which is not an electronic third order nonlinear optical process. It can even overwhelm the electronic contribution to

$\chi_{ijkl}^{(3)}(-\omega;\omega,\omega,-\omega)$ [64]. However, this thermal grating contribution only occurs in the

xxxx configuration where the two probe beams have the same polarization, but does not

occur in the *xyyx* configuration [65,66]. Therefore, to measure the electronic

$\chi_{ijkl}^{(3)}(-\omega;\omega,\omega,-\omega)$ we will use the *xyyx* configuration (see Figure 1.7). The component

we will observe is then $\chi_{xyyx}^{(3)}(-\omega;\omega,\omega,-\omega)$. Because $\chi_{xyyx}^{(3)}(-\omega;\omega,\omega,-\omega)$ is rather small,

its DFWM signal is also small in intensity. Detection of this DFWM signal requires a good

detector sensitivity as well as a high signal to noise ratio.

As indicated, this experimental setup is capable of measuring four components of

the third order nonlinear optical susceptibility tensor. Changing from one configuration to

another can easily be done by changing the half-wave plate angle followed by the polarizer

in the $\mathbf{k}_1$ probe arm.

3.2 DFWM Signal Detection

The first step in studying the dynamics of excited state DFWM is getting the DFWM signal.

This requires good alignment, smooth beam profiles, and, most importantly, an

overlapping, both temporally and spatially, of the two probe beams and the pump beam.

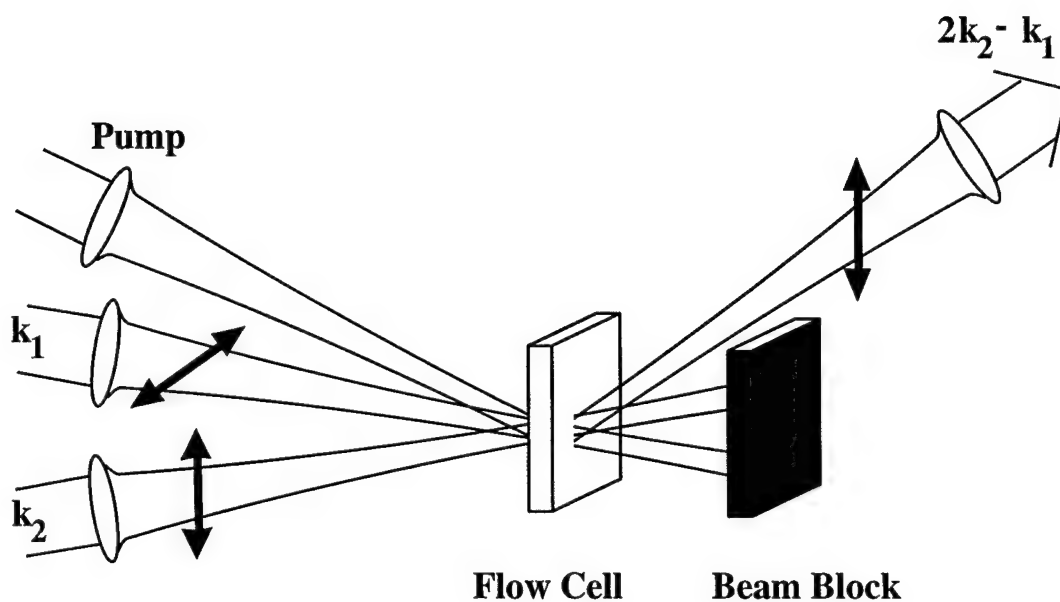The DFWM signal found can then be easily verified by blocking each probe beam and

Figure 1.7 The polarization configuration used in the DFWM experiment. The *xyyx* configuration is set to observe the *xyyx* component of the third order nonlinear optical susceptibility tensor $\chi^{(3)}_{xyyx}(-\omega;\omega,\omega,-\omega)$. The polarizations of the two probe beams are orthogonal to avoid thermal gratings which contribute to the DFWM signal. The k_1 probe is set to be horizontally polarized, while the k_2 probe is vertically polarized. The DFWM signal in the $2k_2$-k_1 direction has the same polarization direction as the k_1 probe. The pump beam polarization has no effect on the DFWM signal.

observing its effect on the DFWM signal, which should be dependent on both of the probe beams. That is, the DFWM signal must vanish when one of the probe beams is blocked. For the case of excited state DFWM, the DFWM signal should drop to the ground state DFWM signal when the pump beam is blocked. The DFWM signal can also be verified by delaying one of the probe beams and observing the effect of delay time on the signal detected. In terms of intensity, the DFWM signal we observe is in the $2\mathbf{k}_2$-$\mathbf{k}_1$ direction and requires two photons from the $\mathbf{k}_2$ probe beam and one photon from the $\mathbf{k}_1$ probe beam, and therefore, the DFWM signal intensities should be dependent on the square of the $\mathbf{k}_2$ beam intensity and linearly on the $\mathbf{k}_1$ beam intensity. By varying the intensities of the two probe beams and monitoring the DFWM signal intensity, we should be able to determine if the signal we detect is the true DFWM signal.

The procedure of detecting the DFWM signal is as follows. First we start with overlapping two probe beams on the sample. Aligning the two probe beams just by eye is not good enough because of the small focal waists of the two probe beams, which are around $100\,\mu$m. The probe beam profiles are shown in Figures 1.8 and 1.9. One important aspect about overlapping the two probe beams is that we have to overlap them both spatially and temporally. Spatial overlap means both probe beams are focused on the same spot on the sample and their beam waists overlap there to create the interaction region. The temporal overlap is the overlap in time domain where the two probe beam pulses must arrive at the interaction region at the same time. Because of the short 30 ps pulse, a good temporal overlap is very crucial to the experiment and any temporal delay between two the probe beams larger than 45 ps, which is the autocorrelation time of two
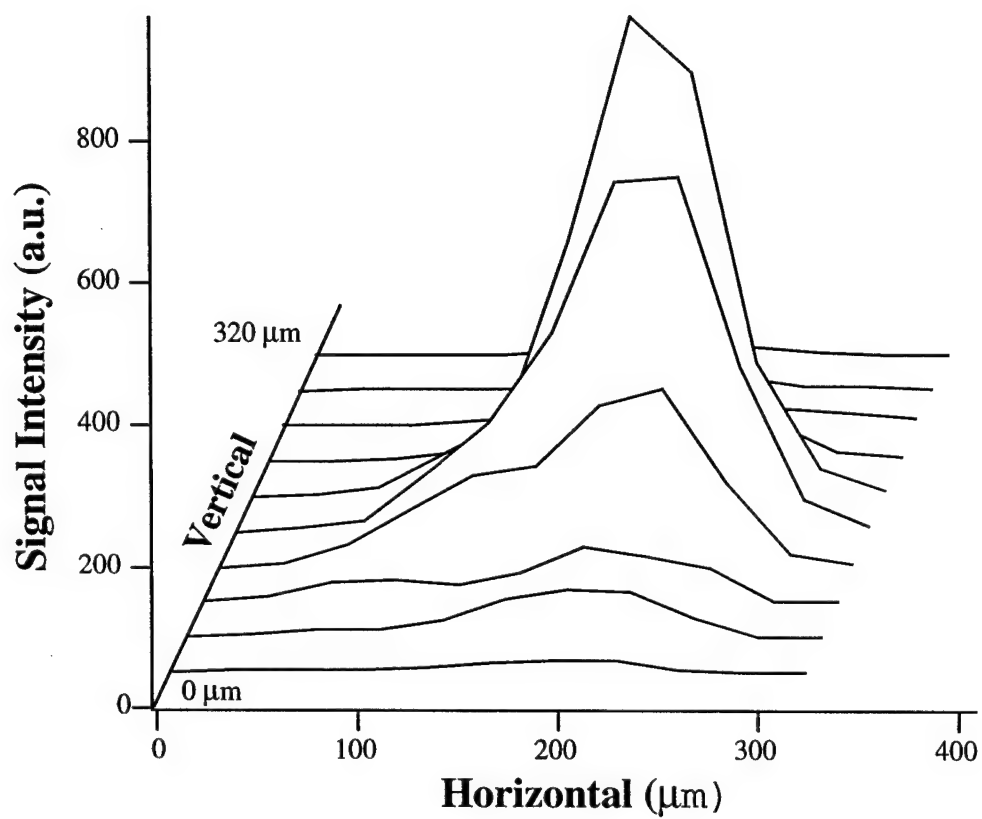
Figure 1.8 The k_1 probe beam profile. The intensity cross section of the k_1 probe is measured at the sample. The FWHM width of the beam is 105 μm.
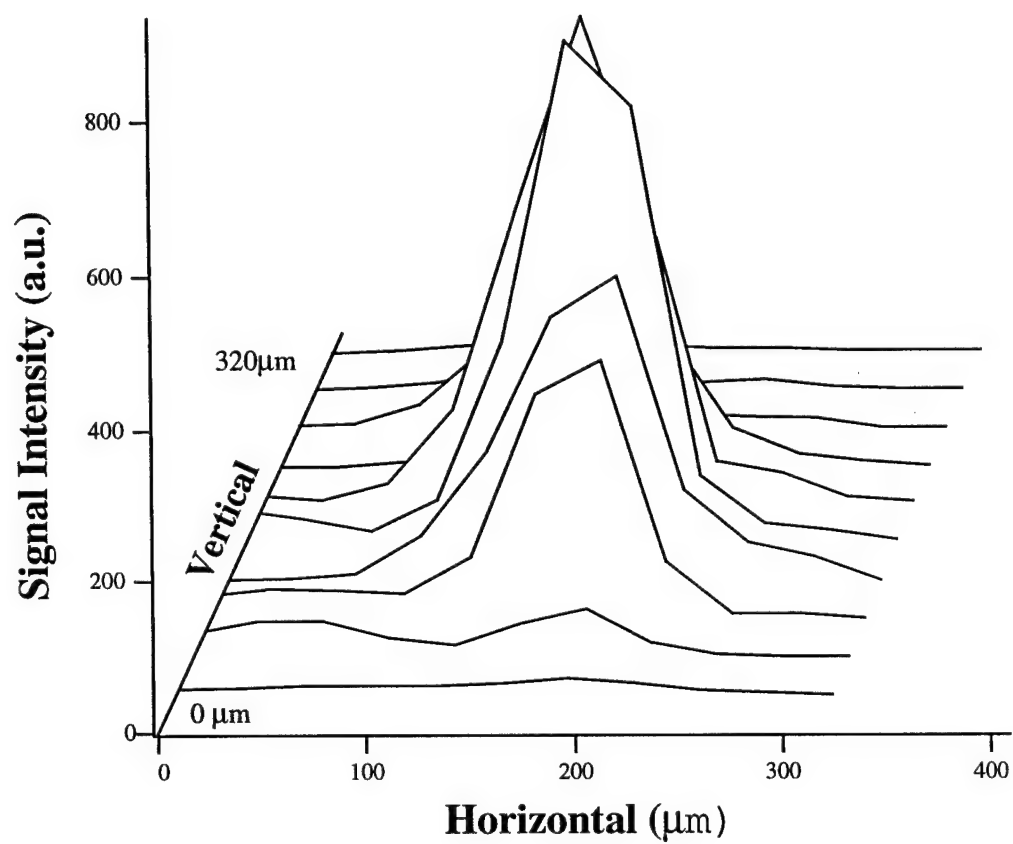
Figure 1.9 The k_2 probe beam profile. The intensity cross section of the k_2 probe is measured at the sample. The FWHM width of the beam is 100 μm.

30 ps gaussian pulses [37], will result in no DFWM signal. In this experiment, both probe beam path lengths are carefully measured, but these measurements are not adequate, since the path length difference has to be less than 1.5 cm in order for the two probe beams to be temporally overlapped. Therefore, we have to find other means to overlap the two probe beams. It is very difficult to match both timing and position simultaneously, because most methods used to match either timing or position require the other to be already matched. To decouple this problem, we first remove the problem of spatial overlap by using bigger beam waists for both probe beams, so that their positions can be easily overlapped by eye using an infrared indicator card. As mentioned before, the time difference is reduced by carefully measuring the path length of each probe beam. To perfectly match the arrival times of the two probes as well as get them to spatially overlap, the TPSA technique is used [67]. In this technique, the 1064 nm laser mode-locking dye is used as the sample. This dye has the useful characteristic that its absorption can easily be saturated by the 30 ps, 1064 nm pulses. To employ this technique, one of the probe beams is used as a pump and the other is used as a probe, with an intensity of approximately 1% of the pump beam. The path lengths of the two beams, therefore, can be matched by monitoring the transmission of the weak probe beam while adjusting the pump beam translation stage and looking for the maximum in the transmission change. The transmission of the weak probe as a function of time is shown in Figure 1.10. When the pump and the probe beams arrive at the mode-locking dye at the same time, the transmission of the weak probe is maximum because the absorption   of   the   dye   is
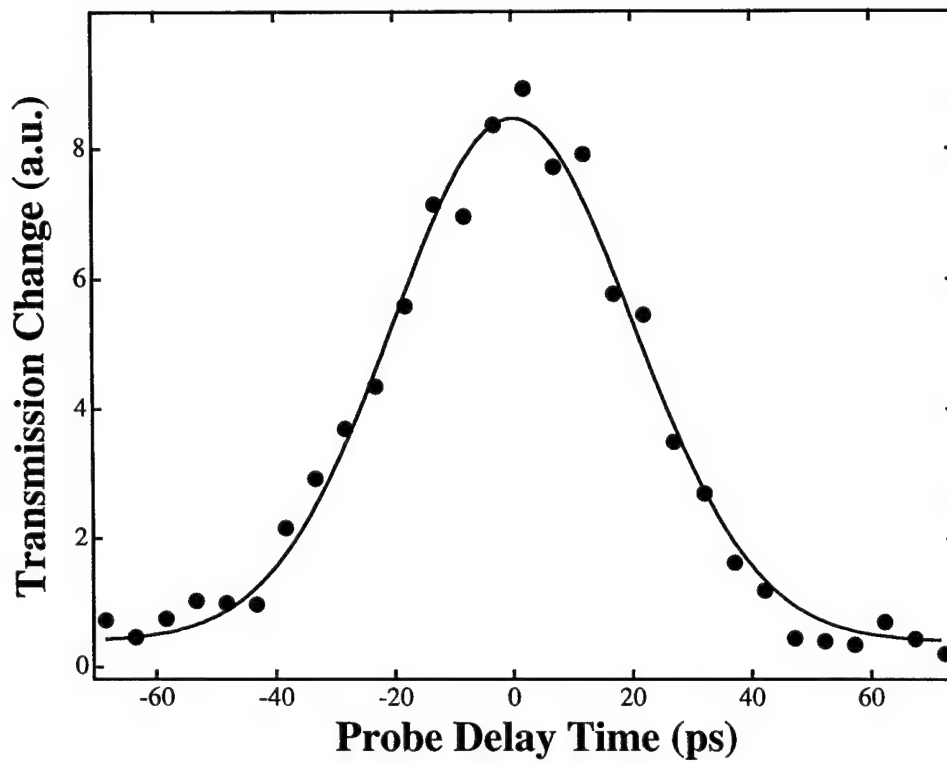
Figure 1.10 The pump-probe transient transmission of mode-locking dye. The pump-probe transient saturable absorption technique is used to match the arrival times at the sample of the two probe beams in the DFWM experiment. In this technique, the k_1 probe is weaker in intensity and is used as a weak probe beam while k_2 is used as a pump beam. The transmission is maximum when the pump and probe are overlapped in time.

saturated by the pump beam. When the weak probe beam arrives after the pump beam its transmission is determined by the decay of the mode-locking dye excited states. For this dye, the lifetime is around 30 ps, and therefore, the decay of the transmission is the same as the pulse width. The same argument cannot be used when the probe precedes the pump because the decay could not occur backward in time. The shape of the transmission on the negative probe delay time is due to the rising time of the pump beam, which is also the pulse width. Therefore, transmission at the negative probe delay time is the autocorrelation of two 30 ps pulses.

Once the time overlap is set we can improve the spatial overlap. We will use the same TPSA technique, but now both beams are focused to beam waists around 100 μm, which is the size we eventually use for the DFWM experiment. By monitoring the transmission of the weak probe beam, while adjusting the pump beam steering mirror, the spatial overlap can be found when the transmission is maximum.

Since the alignment obtained from the TPSA technique is not quite the exact alignment for DFWM, it is useful to try to detect the DFWM signal with a material that has a high $\chi^{(3)}_{xyyx}(-\omega;\omega,\omega,-\omega)$ before using the DPH sample, which has a low $\chi^{(3)}_{xyyx}(-\omega;\omega,\omega,-\omega)$. Carbon disulfide (CS$_2$), with its high $\chi^{(3)}_{xyyx}(-\omega;\omega,\omega,-\omega)$ of $3.6 \pm 0.1 \times 10^{-13}$ esu, is an excellent choice. Because $\chi^{(3)}_{xxxx}(-\omega;\omega,\omega,-\omega)$ is usually higher than $\chi^{(3)}_{xyyx}(-\omega;\omega,\omega,-\omega)$, one could, in principle, use the *xxxx* configuration to find the signal from $\chi^{(3)}_{xxxx}(-\omega;\omega,\omega,-\omega)$ first, and then change to the *xyyx* configuration by rotating the polarizer on the k_1 probe beam arm. However, the alignment change caused by rotating the polarizer makes it very difficult to change from one configuration to another. Since we will use the *xyyx* configuration to study the dynamics of the DFWM, we decided

to use only the *xyyx* configuration for all these preliminary findings. After some adjustment to the spatial overlap, the DFWM signal from CS_2 is found. The DFWM signal is verified by delaying the $\mathbf{k}_1$ probe with respect to the $\mathbf{k}_2$ probe. As we can see from Figure 1.11, the DFWM signal is maximized at zero probe delay time and the signal goes to zero when the two probes are apart more than the pulse width. This probe-probe delay measurement also gives us the exact temporal overlap between the $\mathbf{k}_1$ and the $\mathbf{k}_2$ probes, which occurs at the maximum of the DFWM signal.

The next step is getting the DFWM signal from DPH solution in dioxane. Dioxane is used because it is a good solvent for DPH. In addition, DPH in dioxane has a long fluorescence lifetime of 7.8 ns and should be easily to detect. Observing the DFWM signal while changing the sample from CS_2 to DPH is very difficult because DPH has a very low ground state $\gamma^{S_0}(-\omega;\omega,\omega,-\omega)$, even lower than $\gamma^{Dioxane}(-\omega;\omega,\omega,-\omega)$. Furthermore, the DFWM signal is critically dependent on the alignment and the alignment for CS_2, which has a very high $\chi_{xyyx}^{CS_2}(-\omega;\omega,\omega,-\omega)$, may not be the same as for DPH. In other words, changing from CS_2 to DPH requires an adjustment in alignment as well as cell orientation. The DFWM signal, thus measured, was very small with an extremely low signal to noise ratio due to high background scattering. Practically, the background scattering can be largely reduced by changing the sample cell orientation. However, changing the cell orientation also affects the overlap of the two probe beams. Therefore,
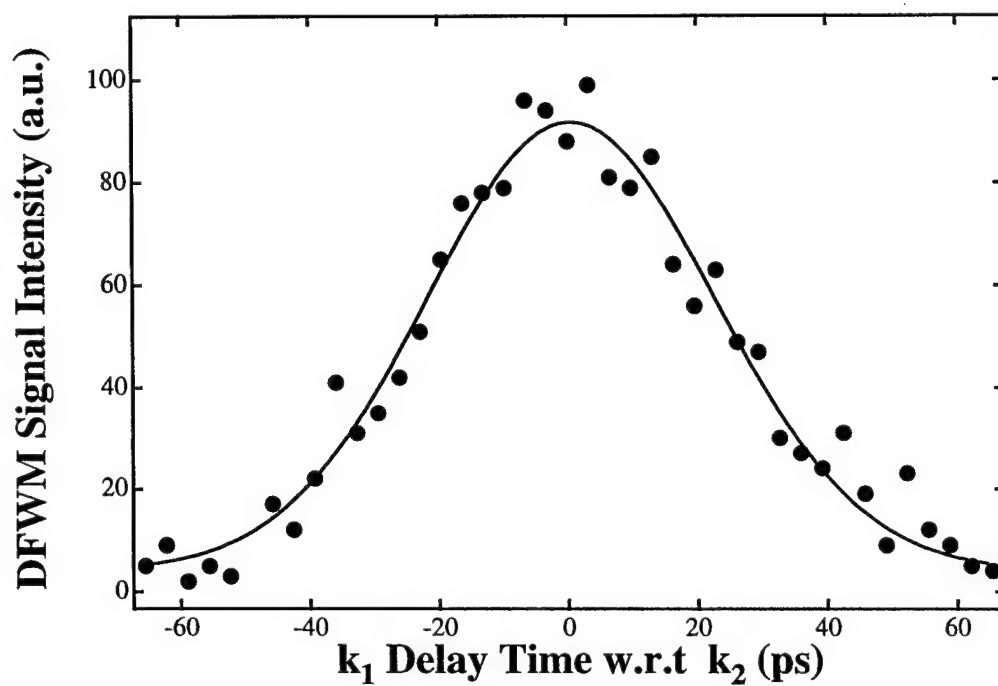
Figure 1.11 Probe delayed DFWM signal of CS_2. CS_2 is used as sample to find the DFWM signal in the *xyyx* configuration. The k_1 probe is delayed with respect to the k_2 probe. The signal is maximum at zero delay time.

we decided to detect the excited state DFWM signal first, by pumping the DPH sample to its excited state using the 355 nm pump beam, and then detecting the signal. As the result, overlap of the pump beam and probe beams is necessary as well. The same rule applies here as in the case of overlapping the two probe beams, that is, the pump and the probe beams must overlap both in space and in time. Because of the long lifetime of DPH in dioxane, the temporal overlap is not as critical as it is in overlapping the two probe beams. The excited state DFWM signal should be seen as long as there are enough molecules in their excited states. This means that the 355 nm pump beam pulse can arrive at the sample up to 1 ns (30 cm) earlier than the two probe beams. However, because it still has a fast rise time, the pump beam cannot follow the probe beam. Careful measurements of the pump and probe beam path lengths are sufficient for the temporal overlap. In order to spatially overlap the pump and the two probe beams, we fix the k_2 probe alignment and then overlap the pump beam on the k_2 probe beam by using a bigger pump beam waist (approximately 3-4 times larger than the probe beam waist, done by moving the pump lens closer to the sample cell). Then, the k_1 probe beam steering mirror is adjusted until the excited state DFWM signal is detected. After the DFWM signal is found, the position of all the apertures that isolate the DFWM signal from scattering are adjusted to optimize the signal. The pump beam lens is then moved back to achieve the smaller pump beam waist, which is around 120 μm (see Figure 1.12), and then scanned for the maximum pump-induced DFWM signal. The pump-induced DFWM signal is verified by delaying the k_1 probe with respect to the k_2 probe (see Figure 1.13).
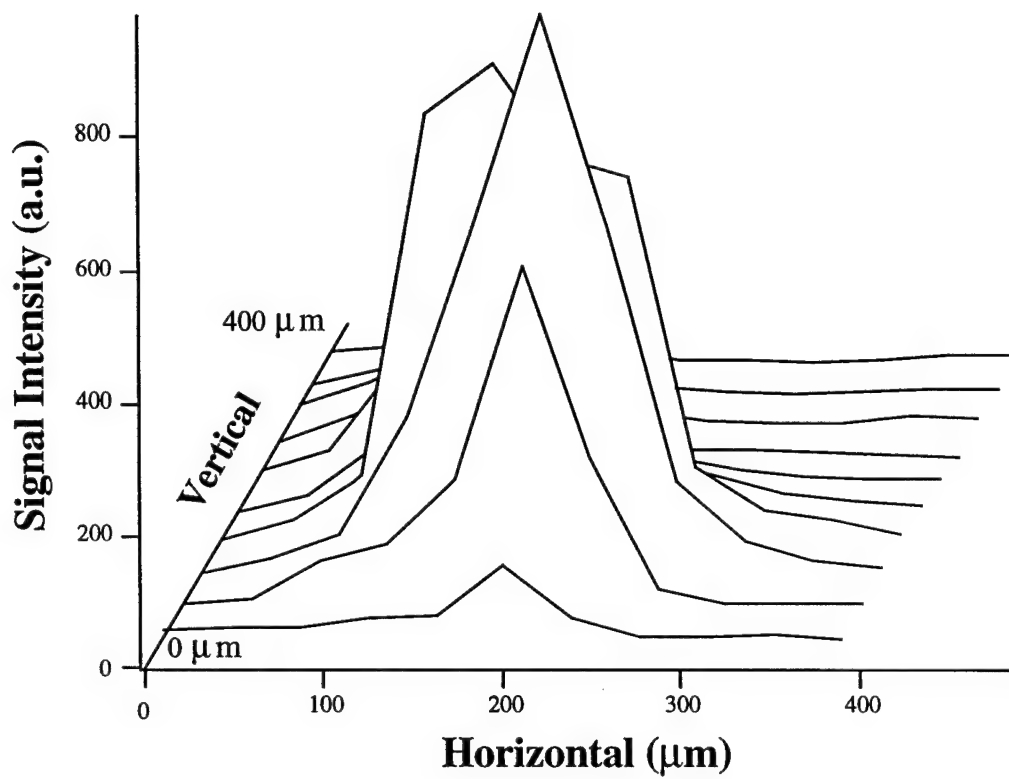
Figure 1.12 The 355 nm pump beam profile. The intensity cross section of the pump beam is measured at the sample. The fwhm width of the beam is 120 μm
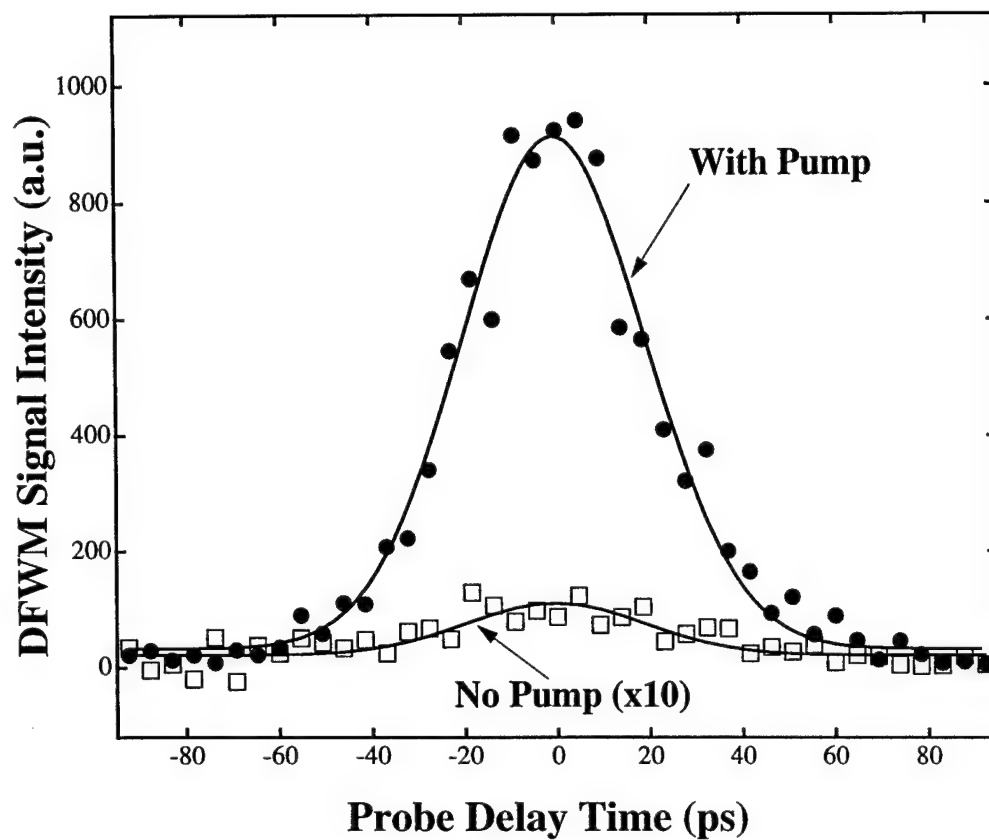
Figure 1.13 Probe delayed DFWM signal in DPH. Both pumped and unpumped signal vanish when the probe delayed time is more than 45 ps.

3.3 Calibration of the Third Order Nonlinear Susceptibility

In this experiment, all the DFWM signal intensities measured are relative values, which means that the values of $\chi^{(3)}_{xyyx}(-\omega;\omega,\omega,-\omega)$ are relative as well. In order to calibrate the $\chi^{(3)}_{xyyx}(-\omega;\omega,\omega,-\omega)$, the DFWM signal intensities of DPH solution are compared to that of CS_2. CS_2 is widely used as a standard for calibration of the third order nonlinear optical susceptibility [63]. Its $\chi^{(3)}_{ijkl}(-\omega;\omega,\omega,-\omega)$ has been extensively studied [68]. The $xyyx$ component is

$$\chi^{(3)}_{xyyx\,CS_2}(-\omega;\omega,\omega,-\omega) = 3.6 \pm 0.1 \times 10^{-13}\,esu \tag{1.3}$$

This value, in our convention, is converted from [68] where

$$24c_{xyyx\,CS_2} = 857 \pm 25 \times 10^{-14}\,esu \tag{1.4}$$

Therefore, experimentally, we need only the ratio between the $xyyx$ component of the third order nonlinear optical susceptibility of DPH and CS_2

$$ratio = \frac{\chi^{(3)}_{xyyx\,CS_2}}{\chi^{(3)}_{xyyx\,DPH}}. \tag{1.5}$$

To measure this ratio, the DFWM signal intensities of DPH was measured in various solvents of concentration 1.0 mmolar with the pump beam present and arriving at the sample at the same time as the probe beam. Then the DPH solutions were replaced with CS_2 without changing any alignment, and the DFWM intensity of CS_2 was measured. The pumped DFWM signal intensity was used because the ground state (unpumped) DFWM signal of DPH in most of the solvents were very low. Since the measured DFWM signal intensities are proportional to the square of $\chi^{(3)}_{xyyx}(-\omega;\omega,\omega,-\omega)$, $\chi^{(3)}_{xyyx\,DPH}(-\omega;\omega,\omega,-\omega)$ can be expressed by

$$\chi^{(3)}_{xyyx\,DPH(With\,Pump)} = \left[\frac{I_{DPH(With\,Pump)}}{I_{CS_2}}\right]^{\frac{1}{2}} \chi^{(3)}_{xyyx\,CS_2} \qquad (1.6)$$

The values of $\chi^{(3)}_{xyyx}(-\omega;\omega,\omega,-\omega)$ of DPH in various solvents are shown in Table 1.1. $\chi^{(3)}_{xyyx}(-\omega;\omega,\omega,-\omega)$ are due to the $\gamma^{S_n}(-\omega;\omega,\omega,-\omega)$ of the ground state and excited state of DPH, as well as the susceptibility of the solvent. This $\chi^{(3)}_{xyyx}(-\omega;\omega,\omega,-\omega)$ can be expressed in terms of $\gamma^{S_n}(-\omega;\omega,\omega,-\omega)$ as follow:

$$\chi^{(3)}_{xyyx}(-\omega;\omega,\,\omega,-\omega) = \frac{1}{3}f_\omega^4\left[\gamma^{Solvent}(-\omega;\omega,\omega,-\omega)N_{Solvent}\right.$$
$$\left. +\gamma^{G.S}(-\omega;\omega,\omega,-\omega)N_{G.S.} + \gamma^{E.S}(-\omega;\omega,\omega,-\omega)N_{E.S.}\right] \qquad (1.7)$$

where $f_\omega = \dfrac{n^2+2}{3}$, is the Lorentz-Lorenz local field factor [69], $\gamma^{G.S.}(-\omega;\omega,\omega,-\omega)$ and $\gamma^{E.S.}(-\omega;\omega,\omega,-\omega)$ are the microscopic isotropically third order nonlinear optical susceptibilities of DPH in the ground state and the excited state, respectively. Because the DFWM signal are observed at $t=0$, i.e., the pump beam is temporally overlapped with the probe beams, only S_0 and S_2 are populated. Therefore equation 1.7 can be written as

$$\chi^{(3)}_{xyyx}(-\omega;\omega,\omega,-\omega) = \frac{1}{3}f_\omega^4\left[\gamma^{Solvent}(-\omega;\omega,\omega,-\omega)N_{Solvent}\right.$$
$$\left. +c\rho_g N_A\gamma^{S_0}(-\omega;\omega,\omega,-\omega)+c\rho_e N_A\gamma^{S_2}(-\omega;\omega,\omega,-\omega)\right] \qquad (1.8)$$

where c is the concentration of the DPH sample, N_A is Avogadro number, and ρ_g and ρ_e are the number densities of the S_0 and S_2 states, respectively. The measured values of $\chi^{(3)}_{xyyx}(-\omega;\omega,\omega,-\omega)$ with and without pump present for DPH in methylcyclohexane of

Sample	$\chi^{(3)}_{xxxx}(-\omega;\omega,\omega,-\omega)$ (x10^{-15} esu.)
Carbon disulfide	357.10
DPH in acetonitrile	20.03
DPH in methylpentane	24.36
DPH in methylcyclohexane	24.50
DPH in dioxane	16.92
DPH in carbon tetrachloride	21.34

Table 1.1 The macroscopic third order nonlinear optical susceptibility $\chi^{(3)}_{xyyx}(-\omega;\omega,\omega,-\omega)$ are shown for carbon disulfide, and DPH in various solvents of concentration 1 mmolar. CS_2 is used as to calibrate the macroscopic susceptibility $\chi^{(3)}_{xyyx}(-\omega;\omega,\omega,-\omega)$ of DPH solutions by comparing the DFWM signal intensities which are proportional to the squared $\chi^{(3)}_{xyyx}(-\omega;\omega,\omega,-\omega)$.

different concentrations are shown in Figure 1.14. When the pump is present there is a

nonzero ρ_e and the slope of the curve can be derived from equation 1.8 as

$$\frac{\partial \chi_{xyyx}^{(3)}(-\omega;\omega,\omega,-\omega) \ With \ Pump}{\partial c} = \frac{1}{3} f_\omega^4 [\rho_g N_A \gamma^{S_0}(-\omega;\omega,\omega,-\omega)$$
$$+\rho_e N_A \gamma^{S_2}(-\omega;\omega,\omega,-\omega)]$$

$$(1.9)$$

When there is no pump present, $\rho_e = 0$ and the slope for the unpumped

$\chi_{xyyx}^{(3)}(-\omega;\omega,\omega,-\omega)$ is

$$\frac{\partial \chi_{xyyx}^{(3)}(-\omega;\omega,\omega,-\omega) \ No \ Pump}{\partial c} = \frac{1}{3} f_\omega^4 \rho_g N_A \gamma^{S_0}(-\omega;\omega,\omega,-\omega) \qquad (1.10)$$

From the graph, this slope is close to zero, indicating that the unpumped DFWM signal is

independent of the concentration. It means that $\gamma^{S_0}(-\omega;\omega,\omega,-\omega)$ of DPH is smaller than

the experimental resolution of $\pm 200 \times 10^{-36}$ esu, and the unpumped signal is entirely

contributed by the solvent. Using this argument and equation 1.9, we arrive at the

expression for $\gamma^{S_2}(-\omega;\omega,\omega,-\omega)$:

$$\gamma^{S_2}(-\omega;\omega,\omega,-\omega) = \frac{3}{f_\omega^4 \rho_e N_A} \frac{\partial \chi_{xyyx}^{(3)}(-\omega;\omega,\omega,-\omega) \ With \ Pump}{\partial c} \qquad (1.11)$$

Both pumped and unpumped $\chi_{xyyx}^{(3)}(-\omega;\omega,\omega,-\omega)$ curves intersect the y-axis at the same

point, and this y-intercept is the third order nonlinear optical susceptibility of the solvent

$\chi_{xyyx \ Solvent}^{(3)}(-\omega;\omega,\omega,-\omega)$. The values of $\gamma^{S_2}(-\omega;\omega,\omega,-\omega)$ of DPH in various solvents
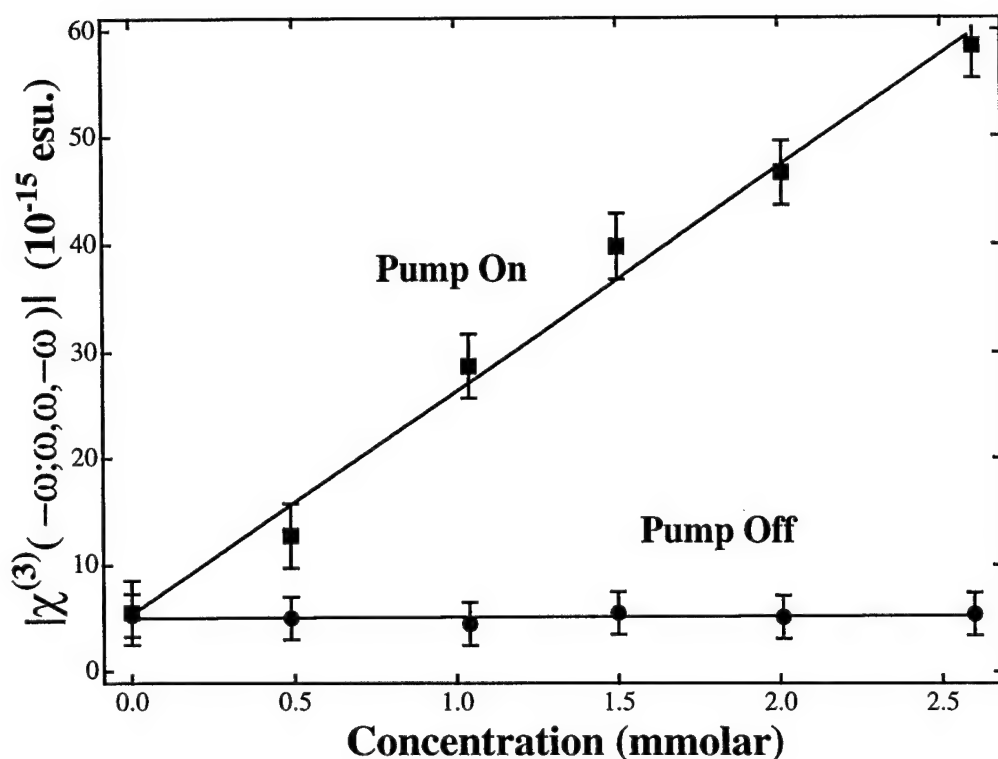
are shown in Table 1.2

Figure 1.14 Concentration dependence of $\chi^{(3)}_{xyyx}(-\omega;\omega,\omega,-\omega)$. The values of $\chi^{(3)}_{xyyx}(-\omega;\omega,\omega,-\omega)$ for DPH solutions in methylcyclohexane are shown here as a function of solution concentration. The pump on data are the values of $\chi^{(3)}_{xyyx}(-\omega;\omega,\omega,-\omega)$ from the DFWM signal when the pump is present, and the pump off data are the values of $\chi^{(3)}_{xyyx}(-\omega;\omega,\omega,-\omega)$ when no pump is present. The slope of the upper line is directly proportional to the excited state molecular susceptibility $\gamma^{S_2}(-\omega;\omega,\omega,-\omega)$. The lower line slope corresponds to the ground state molecular susceptibility $\gamma^{S_0}(-\omega;\omega,\omega,-\omega)$. Its zero value gives an upper bound of 200×10^{-36} esu for DPH $\gamma^{S_0}(-\omega;\omega,\omega,-\omega)$. The unpumped $\chi^{(3)}_{xyyx}(-\omega;\omega,\omega,-\omega)$, therefore, is due to the solvent.

Solvent	$\gamma_{DPH}^{S_2}(-\omega;\omega,\omega,-\omega)$ (x10^{-36} esu.)
Acetonitrile	57900 ± 4500
Methylpentane	60900 ± 4500
Methylcyclohexane	60300 ± 4500
Dioxane	49200 ± 4500
Carbon tetrachloride	41700 ± 4500

Table 1.2 The values of the S_2 excited state molecular susceptibility $\gamma^{S_2}(-\omega;\omega,\omega,-\omega)$ of DPH in solvents are calculated from the concentration dependent $\chi_{xyyx}^{(3)}(-\omega;\omega,\omega,-\omega)$.

4.0 Dynamics of Excited State DFWM

4.1 Introduction

To study the dynamics of the excited state DFWM, the time difference between the pump beam and the probe beams is needed. This can be done by either changing the path length of the pump or the probe beams (the path lengths of the two probe beams must be equal for maximum DFWM signal). Practically, it is much easier to change the path length of the pump beam while maintaining the path length of the DFWM probe beams because we then have to adjust the alignment of only one beam. In addition, keeping the path length of the two probe beams constant assures us that the overlapping of two probe beams, which is very critical to the DFWM signal intensity, is exactly the same for every delay position. By observing the DFWM signal intensities for many pump probe delay times, we measure the time decay of the excited state population responsible for the enhancement of $\chi^{(3)}_{xyyx}(-\omega;\omega,\omega,-\omega)$. Because a long lifetime of the excited state of DPH is expected, path length variations of 2 m are necessary. This can be done by using a motorized translation stage on a 1-meter rail. It is very crucial that the pump and probe beams are always overlapped on the sample. To avoid having to realign the pump beam position on the sample at each delay position, the retroreflector (corner cube) is used to reflect the pump beam from the translation stage. This retroreflector fixes the pump beam position on the sample while the pump beam path length is varied. Alignment using the retroreflector is much better than that using mirrors or prisms. In order to verify that the pump-probe beam overlapping is always achieved, the pump lens that focuses and positions the pump beam on the sample is scanned for the largest pump induced DFWM signal. The pump lens is

located after the optical delay line and before the sample cell, so any misalignment caused by translation of the pump delay stage can be compensated by repositioning the pump lens. The peak amplitude of such a scan on each delay is always on the origin, which means that moving the translation stage does not change the pump beam position on the sample at all.

The technique involved in the study of the dynamics of the DFWM process is similar to TPSA, which was discussed in chapter 5. In TPSA, the transmission of the probe beam is monitored with respect to the pump-probe delay time. When the probe beam follows the pump beam in time, it encounters a mixture of molecules in their ground states and excited states, and therefore, measures absorption different from the ground state absorption. Similarly, in the case of DFWM, when the two probe beams precede the pump beam, they encounter only molecules in the ground state, and the DFWM signal is produced by the ground state molecules. In contrast, when the probes follow the pump beam, they encounter mixtures of molecules in both excited state and ground state, and the DFWM signal in this case is produced by a susceptibility that is a sum of contributions from the excited and ground state molecules. As indicated in [9], $\gamma^{S_2}(-\omega;\omega,\omega,-\omega)$ is orders of magnitude higher than $\gamma^{S_0}(-\omega;\omega,\omega,-\omega)$, so the DFWM signal is expected to decay as the excited state population decreases with increasing delay time.

4.2 Experimental Results

In order to completely test the dynamical model, a wide range of energy gaps ΔE is used in studying the time evolution of the DFWM signal from the DPH samples. The same solvents used in the TPSA experiments are used for the DFWM experiments. They are 1,4-dioxane, acetonitrile, carbon tetrachloride, methylcyclohexane and 3-methylpentane. They are chosen because they give a variety of ΔE as well as the lifetimes that we need for the study. These solvents have reasonably high boiling points so they will not easily evaporate from the DPH solutions. They also do not directly interact with DPH as some other solvents do (for example, DPH in acetone forms a radical cation, DPH$^+$ [70]). They have no effect on the conformation of DPH. This proves to be the major advantage of using the solvent effect to change the energy gap ΔE, over varying temperature, because when DPH is heated up its conformation can change from all-trans to cis or cis-trans [50]. These changes in conformation, if they occur, will totally complicate the experiment since different conformations have different lifetimes, energy gaps, and other properties. DPH in these solvents has a main absorption peak at around 350 nm, and can be easily pumped to its excited state by a 355 nm beam. Furthermore, DPH dissolves well in these solvents and can reach a concentration of up to 10 mmolar. In this study, low concentration is preferred so that the individual molecule can be considered as independent of other DPH molecules. However, there is a drawback of using samples with low concentration. Because DFWM is a third order nonlinear optical process, in which the signal is normally small, the smaller signal accompanying lower sample concentrations could make detection much more difficult. The concentrations of the DPH solutions used in this experiment are approximately 0.5, 1.0, 1.5, 2.0, and 2.5 mmolar. The exact concentration of each sample

is obtained by measuring the sample absorption at its wavelength maximum and then calculating it from the relation

$$a = c\varepsilon L \tag{1.12}$$

where c is the concentration, a is the absorption, L is the thickness of the cell used in measuring the absorption, and ε is the extinction coefficient for DPH in a given solvent. ε is found from calibration of equation 1.12 using many well measured concentrations. All the solvents used in the experiment are fresh. They are prepared and used on the same day to avoid any change in their properties caused by aging solutions. The DPH used in this study was obtained from Aldrich Chemical Company and used without further purification. Nuclear Magnetic Resonance Scan (NMR) and Differential Scan Calorimetry (DSC) comparisons to 100% all-tran-1,6-diphenyl-1,3,5-hexatriene (purified by vacuum sublimation) show no difference before and after purification. This confirms that the compounds as received were sufficiently pure all-tran-1,6-diphenyl-1,3,5-hexatriene for the experiment. The solvents used are all of spectroscopic grade and were protected from oxidation. The sample bottles are also filled with nitrogen gas, instead of regular air, to prevent the sample from suffering any atmospheric contamination.

Qualitatively, the time evolved $\chi^{(3)}_{xyyx}(-\omega;\omega,\omega,-\omega)$ exhibits two-component exponential decay with two characteristic lifetimes as predicted by the dynamical model. These two lifetimes, a short lifetime, τ_1, which corresponds to the thermal equilibrium of the two excited states, and a long lifetime, τ_2, which corresponds to the decay of both excited states to the ground state, can be retrieved from a two-component exponential fit of the data.

Figures 1.15-1.19 show the time evolution of $\chi^{(3)}_{xyyx}(-\omega;\omega,\omega,-\omega)$ from DPH at all concentrations in dioxane, acetonitrile, methylpentane, carbon tetrachloride, and methylcyclohexane, respectively. All curves exhibit two-component exponential decay with short lifetimes τ_1 and long lifetimes, τ_2, except for DPH in carbon tetrachloride which exhibits single exponential decay due to a very short τ_2. The lifetimes of $\chi^{(3)}_{xyyx}(-\omega;\omega,\omega,-\omega)$ are extracted from these curves using the component-stripping technique discussed in chapter 5 and are shown in Table 1.3. The lifetimes shown are averaged values of lifetimes from all concentrations of DPH solutions since concentration seems to have no or at least little effect on the lifetimes (see Figures 1.20 and 1.21).

To illustrate the solvent effects on the time evolution of $\chi^{(3)}_{xyyx}(-\omega;\omega,\omega,-\omega)$, the time dependent $\chi^{(3)}_{xyyx}(-\omega;\omega,\omega,-\omega)$ of DPH in all solvents at 1.0 mmolar are shown on the same graph (see Figure 1.22). The effects both on the lifetimes and the magnitude of $\chi^{(3)}_{xyyx}(-\omega;\omega,\omega,-\omega)$ are obviously seen in the curves for different solvents, similar to the TPSA results.
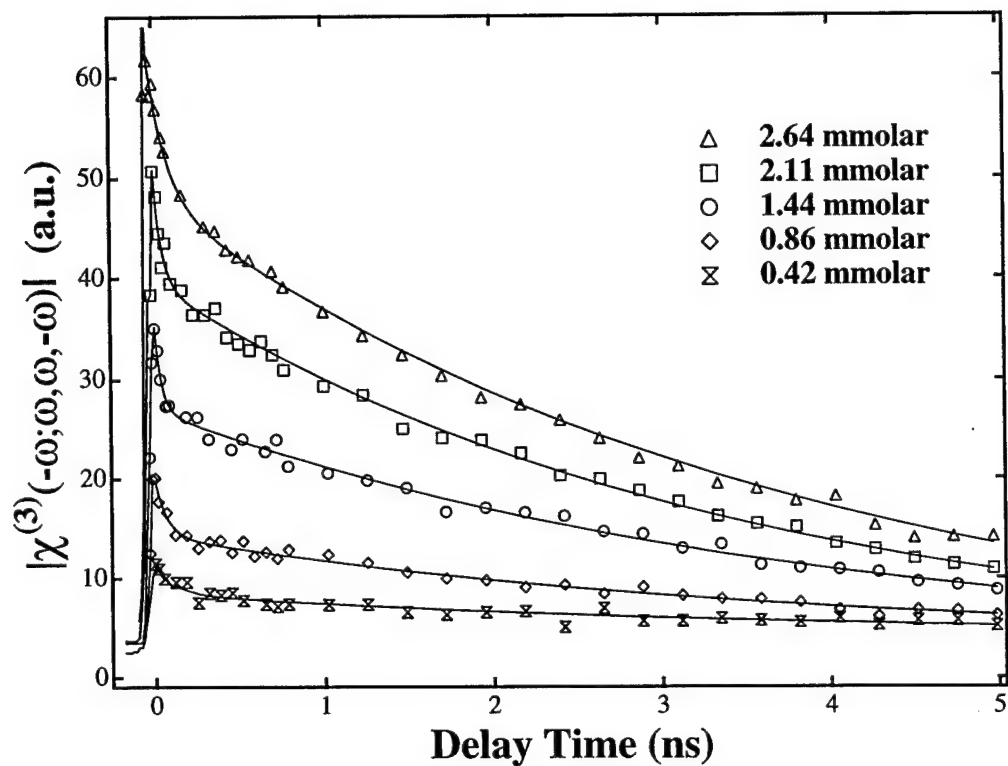
Figure 1.15 Time evolution of $\chi_{xyyx}^{(3)}(-\omega;\omega,\omega,-\omega)$ of DPH in dioxane. The third order nonlinear optical susceptibility, $\chi_{xyyx}^{(3)}(-\omega;\omega,\omega,-\omega)$, of DPH in dioxane at various concentrations exhibits two-component exponential decay.
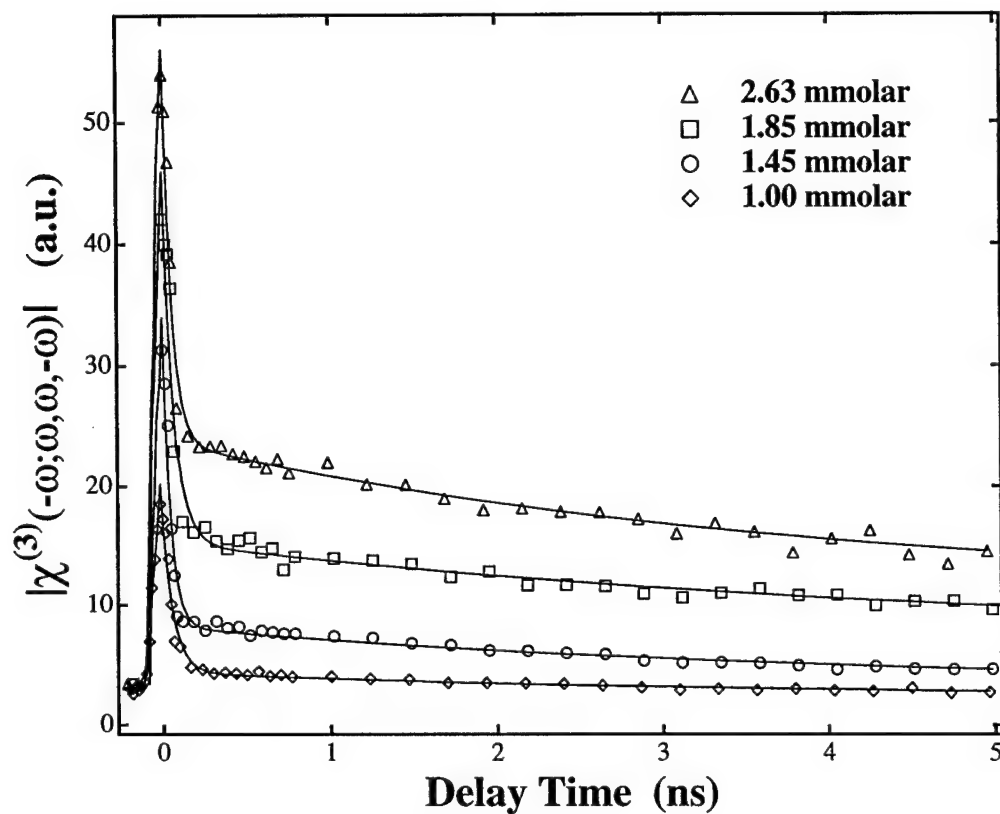
Figure 1.16 Time evolution of $\chi^{(3)}_{xyyx}(-\omega;\omega,\omega,-\omega)$ of DPH in acetonitrile. The third order nonlinear optical susceptibility, $\chi^{(3)}_{xyyx}(-\omega;\omega,\omega,-\omega)$, of DPH in acetonitrile at various concentrations exhibits two-component exponential decay.
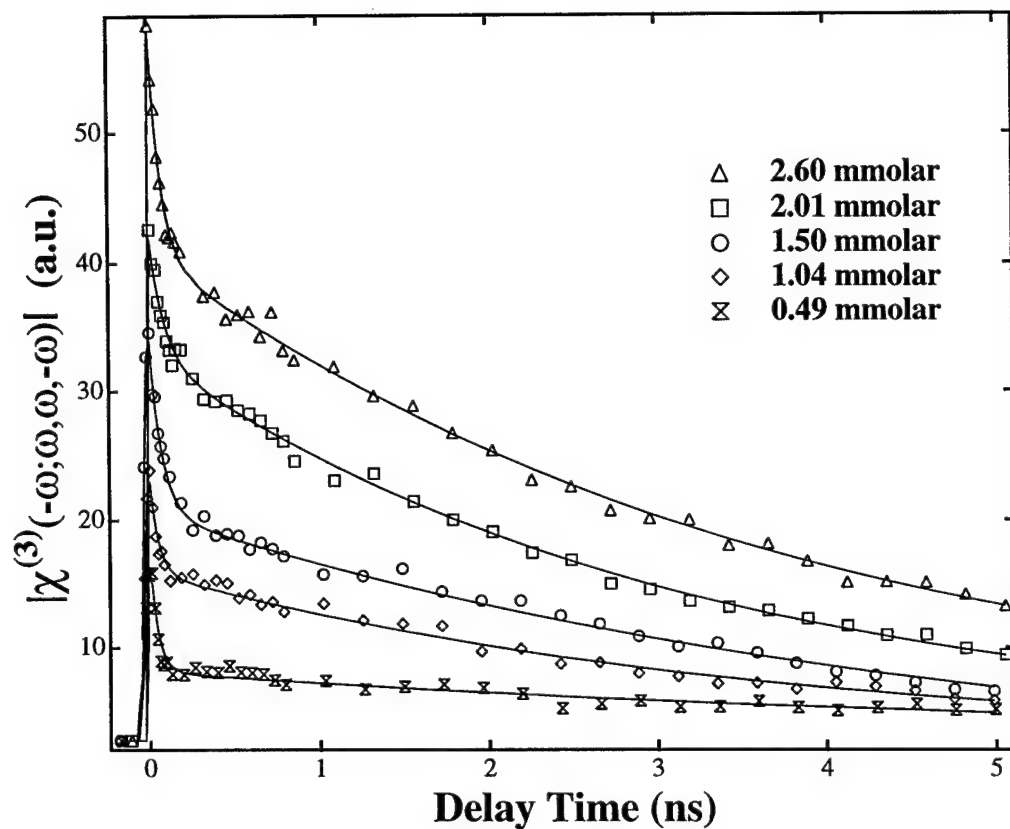
Figure 1.17 Time evolution of $\chi^{(3)}_{xyyx}(-\omega;\omega,\omega,-\omega)$ of DPH in methylcyclohexane. The third order nonlinear optical susceptibility, $\chi^{(3)}_{xyyx}(-\omega;\omega,\omega,-\omega)$, of DPH in methylcyclohexane at various concentrations exhibits two-component exponential decay.

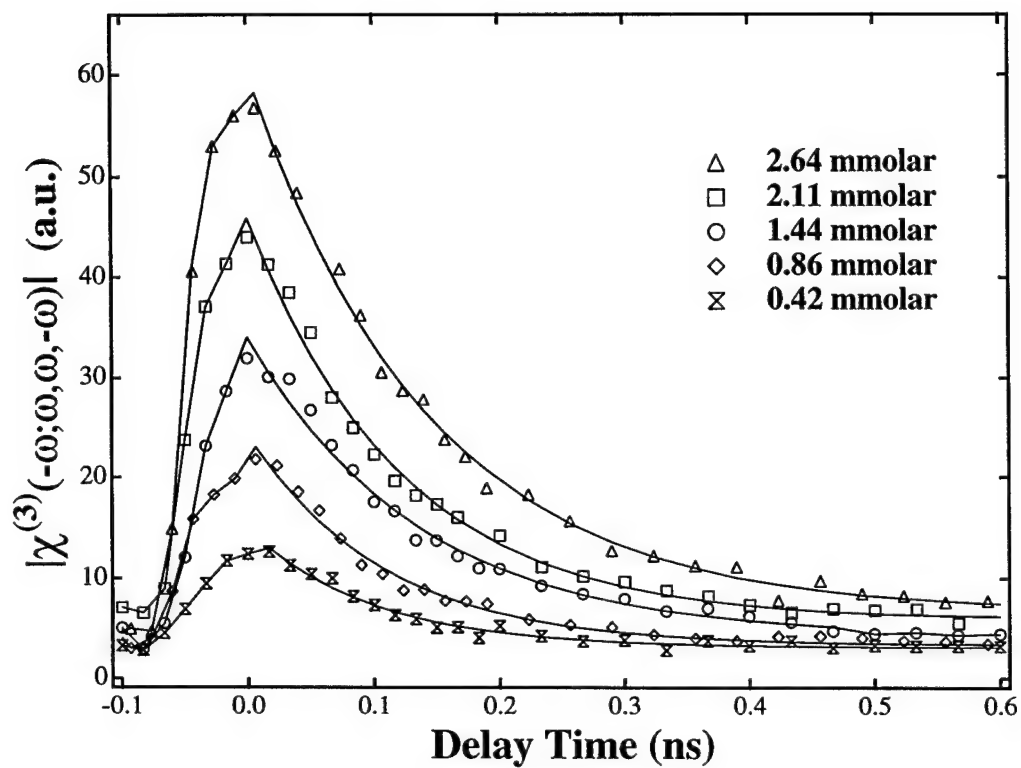Figure 1.18 Time evolution of $\chi^{(3)}_{xyyx}(-\omega;\omega,\omega,-\omega)$ of DPH in carbon tetrachloride. The third order nonlinear optical susceptibility, $\chi^{(3)}_{xyyx}(-\omega;\omega,\omega,-\omega)$, of DPH in carbon tetrachloride at various concentrations exhibits two-component exponential decay.

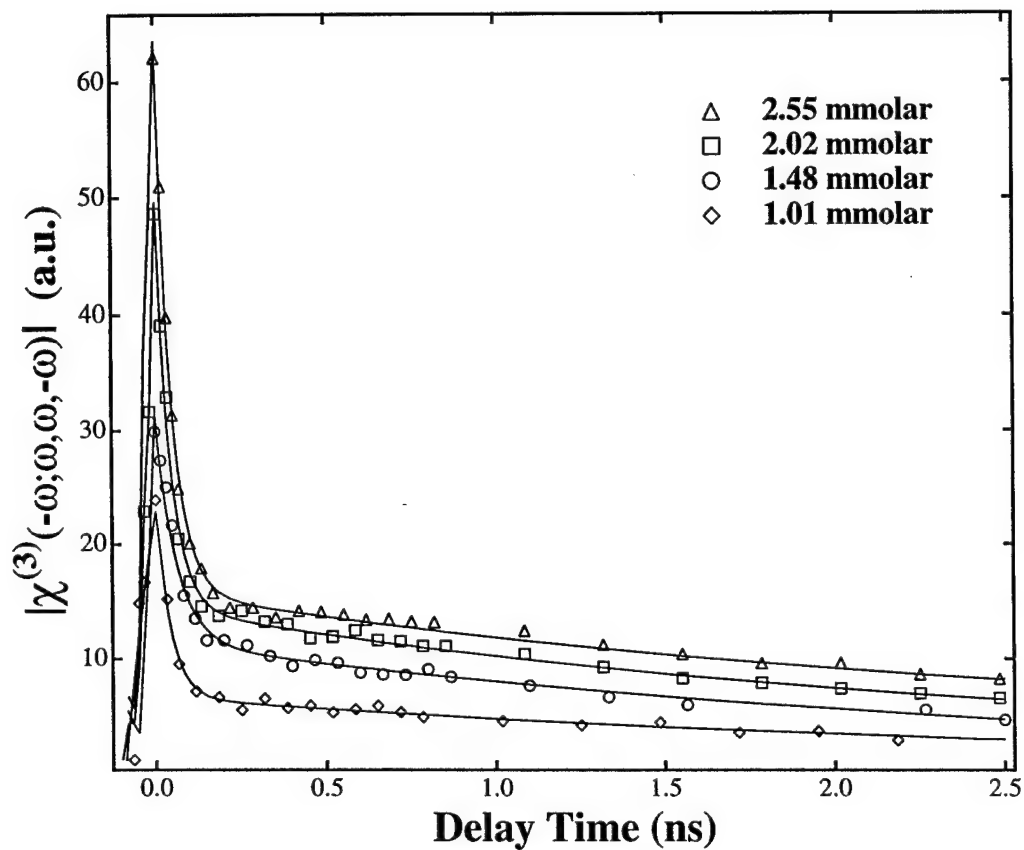Figure 1.19 Time evolution of $\chi^{(3)}_{xyyx}(-\omega;\omega,\omega,-\omega)$ of DPH in methylpentane. The third order nonlinear optical susceptibility, $\chi^{(3)}_{xyyx}(-\omega;\omega,\omega,-\omega)$, of DPH in methylpentane at various concentrations exhibits two-component exponential decay.

Solvent for DPH	Short Lifetime τ_1 (ps)	Long Lifetime τ_2 (ns)
Acetonitrile	52 ± 10	3.9 ± 0.2
Methylpentane	45 ± 10	2.3 ± 0.2
Methylcyclohexane	73 ± 10	3.8 ± 0.2
Dioxane	65 ± 10	3.8 ± 0.2
Carbon tetrachloride	Not Available.	0.11 ± 0.02

Table 1.3 Two characteristic lifetimes, τ_1 and τ_2, of the third order nonlinear optical susceptibility $\chi_{xyyx}^{(3)}(-\omega;\omega,\omega,-\omega)$ of DPH in various solvents. The values are averaged from different concentrations used in the study. The short lifetime, τ_1, corresponds to the time to reach the thermal equilibrium and the long lifetime, τ_2, corresponds to the decay time of both excited states to the ground state.
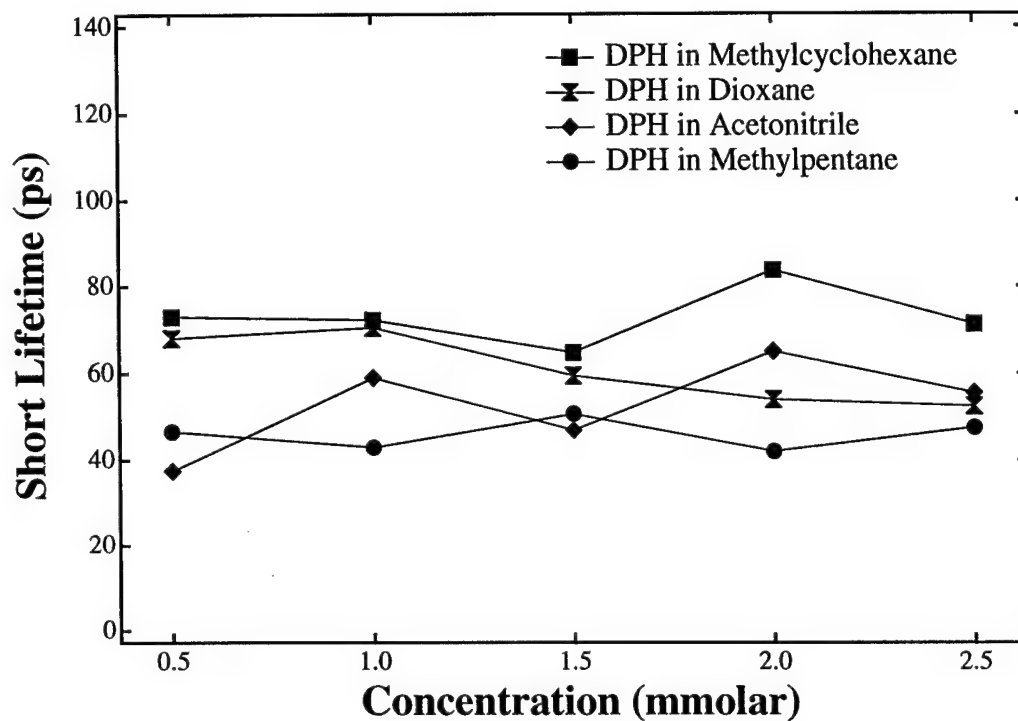
Figure 1.20 The short lifetimes, τ_1, of the excited state enhanced third order nonlinear optical susceptibility, $\chi^{(3)}_{xyyx}(-\omega;\omega,\omega,-\omega)$ in several solvents at different concentrations. The lifetimes are independent of the concentration.

Figure 1.21 The long lifetimes, τ_2, of the excited state enhanced third order nonlinear optical susceptibility, $\chi^{(3)}_{xyyx}(-\omega;\omega,\omega,-\omega)$ in several solvents at different concentrations. The lifetimes are independent of the concentration.
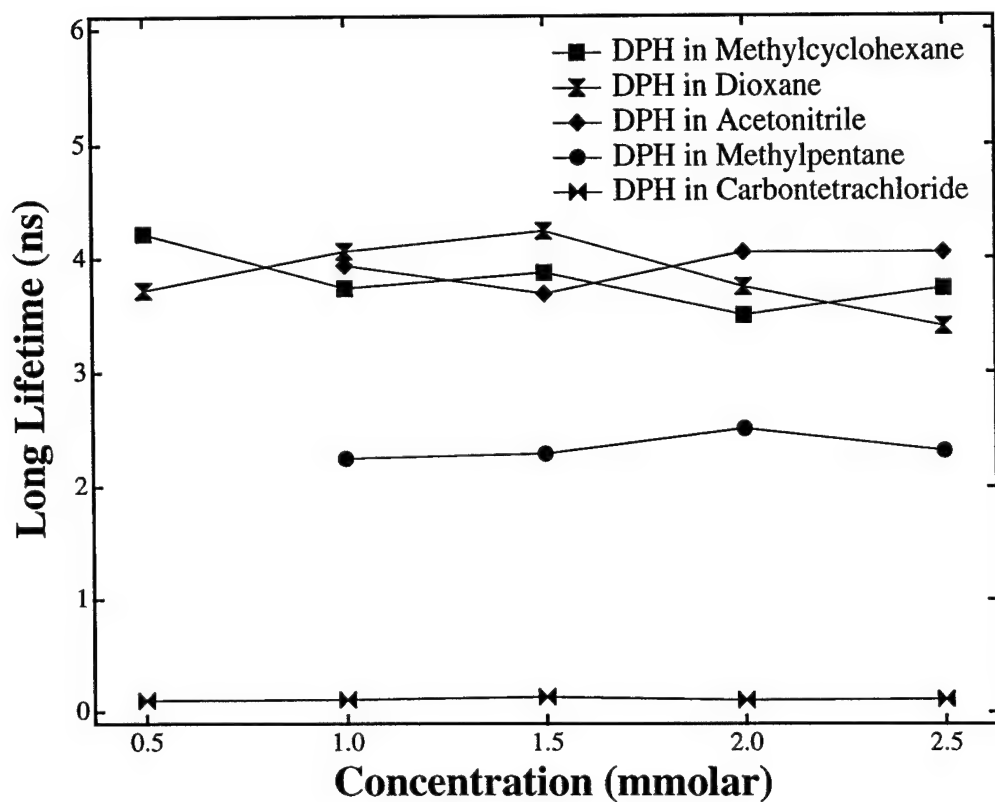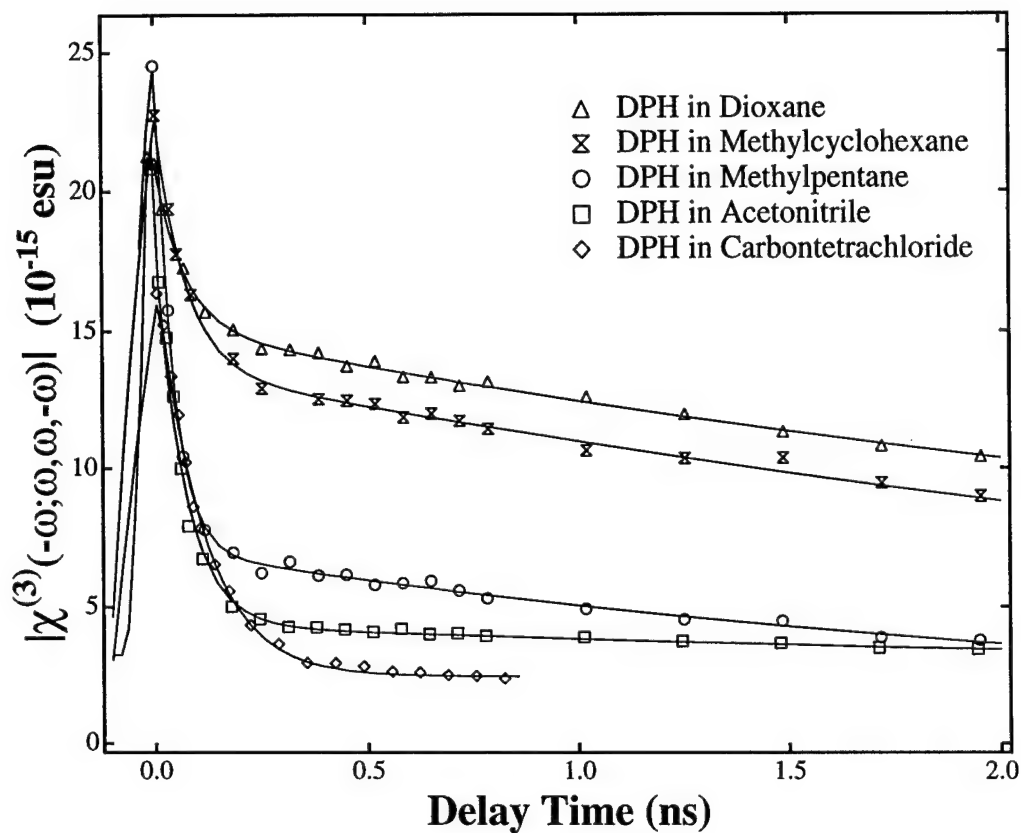
Figure 1.22 Time evolution of $\chi^{(3)}_{xyyx}(-\omega;\omega,\omega,-\omega)$ of DPH in various solvents. The concentrations of all DPH solutions are 1.0 mmolar. Solvent effects on the energy gap result in a variety of lifetimes and magnitude of the time evolved third order nonlinear optical susceptibilities $\chi^{(3)}_{xyyx}(-\omega;\omega,\omega,-\omega)$.

As previously mentioned, values of the energy gaps are needed to determine $\gamma^{S_1}(-\omega;\omega,\omega,-\omega)$. The $\gamma^{S_2}(-\omega;\omega,\omega,-\omega)$ of DPH in all the solvents are already determined from the concentration dependent $\chi^{(3)}_{xyyx}(-\omega;\omega,\omega,-\omega)$ studies in section 1.4.3. The energy gap can be derived from the ratio between B and C in equation 5.25.

$$\chi^{(3)}_{xyyx}(-\omega;\omega,\ \omega,-\omega) = A + B\exp^{-t\,/\,\tau_1} + C\exp^{-t\,/\,\tau_2} \tag{1.13}$$

By neglecting $\gamma^{S_0}(-\omega;\omega,\omega,-\omega)$, since the value is very small compared to $\gamma^{S_2}(-\omega;\omega,\omega,-\omega)$, we get

$$\frac{B}{C} = \frac{\gamma^{S_2}(-\omega;\omega,\omega,-\omega) - \gamma^{S_1}(-\omega;\omega,\omega,-\omega)}{\dfrac{k_{12}}{k_{21}}\gamma^{S_2}(-\omega;\omega,\omega,-\omega) + \gamma^{S_1}(-\omega;\omega,\omega,-\omega)} \tag{1.14}$$

or

$$\frac{B}{C} = \frac{1-\delta}{\exp^{-\Delta E/k_B T} + \delta} \tag{1.15}$$

where δ is defined by

$$\delta = \frac{\gamma^{S_1}(-\omega;\omega,\omega,-\omega)}{\gamma^{S_2}(-\omega;\omega,\omega,-\omega)} \tag{1.16}$$

The ratio $\dfrac{B}{C}$ is obtained from the time dependent $\chi^{(3)}_{xyyx}(-\omega;\omega,\omega,-\omega)$ of DPH in each solvent. However, equation 1.15 still has two variables, ΔE and δ, for each solvent. In order to solve this equation, the assumption that DPH in all solvents has the same $\gamma^{S_1}(-\omega;\omega,\omega,-\omega)$ has been made. This assumption is based on the insensitivity of the S_1 energy level to the solvent polarizability. Since the polarizability of dioxane and methylcyclohexane are very close, their energy gaps are approximately the same

$$\Delta E_{Dioxane} = \Delta E_{Methylcyclohexane} \tag{1.17}$$

This equation is used to determine ΔE and δ of DPH. $\gamma^{S_1}(-\omega;\omega,\omega,-\omega)$ of DPH is determined to be $22,500 \pm 3,000 \times 10^{-36}$ esu. The calculated values of energy gap for DPH in various solvents are shown in Table 1.4. With knowledge of the energy gap, we can look back at Figure 1.22 and see the effect of the energy gap on the magnitude of $\chi^{(3)}_{xyyx}(-\omega;\omega,\omega,-\omega)$ at the nanosecond timescales, since $\chi^{(3)}_{xyyx}(-\omega;\omega,\omega,-\omega)$ is the sum of individual $\gamma^{S_n}(-\omega;\omega,\omega,-\omega)$ weighted by the population densities of each state. There is a greater population in the S_2 state for a smaller energy gap, resulting in higher $\chi^{(3)}_{xyyx}(-\omega;\omega,\omega,-\omega)$ as $\gamma^{S_2}(-\omega;\omega,\omega,-\omega) > \gamma^{S_1}(-\omega;\omega,\omega,-\omega)$.

The two characteristic lifetimes measured by DFWM and TPSA experiments are comparable for DPH in each solvent. The TPSA short lifetimes in all solvents are slightly higher, but their experimental uncertainty is also high as a result of the low coefficients, B, in the expression for $\ln\left[\dfrac{T}{T_o}\right]$ (see equation 5.36). We note that the long lifetimes, τ_2, obtained from the two experiments are lower than the fluorescence lifetimes of DPH in each solvent (see Table 4.1). For an explanation of this behavior, we look back to the dynamical model described in section 5.4.2. The long lifetime τ_2 is not the same as the fluorescence lifetime of the S_1 state, which is $\dfrac{Q_F}{k_1}$. τ_2 is in fact contributed to by decay rates of both $S_2 \rightarrow S_0$ and $S_1 \rightarrow S_0$ transitions as defined by equation 5.14

$$\tau_2 = \frac{k_{12}+k_{21}}{k_1 k_{21}+k_2 k_{12}} \qquad (1.17)$$

Using the value of k_2 and k_1 from the literature [53,56,71] and the energy gaps obtained in our study, the predicted values of τ_2 can be calculated for DPH in each solvent (see

Solvent for DPH	Energy Gap ΔE (cm^{-1})
Acetonitrile	720 ± 90
Methylpentane	470 ± 70
Methylcyclohexane	140 ± 50
Dioxane	140 ± 50
Carbon tetrachloride	<50

Table 1.4 Energy gap ΔE between the S_1 and S_2 states of DPH in various solvents.
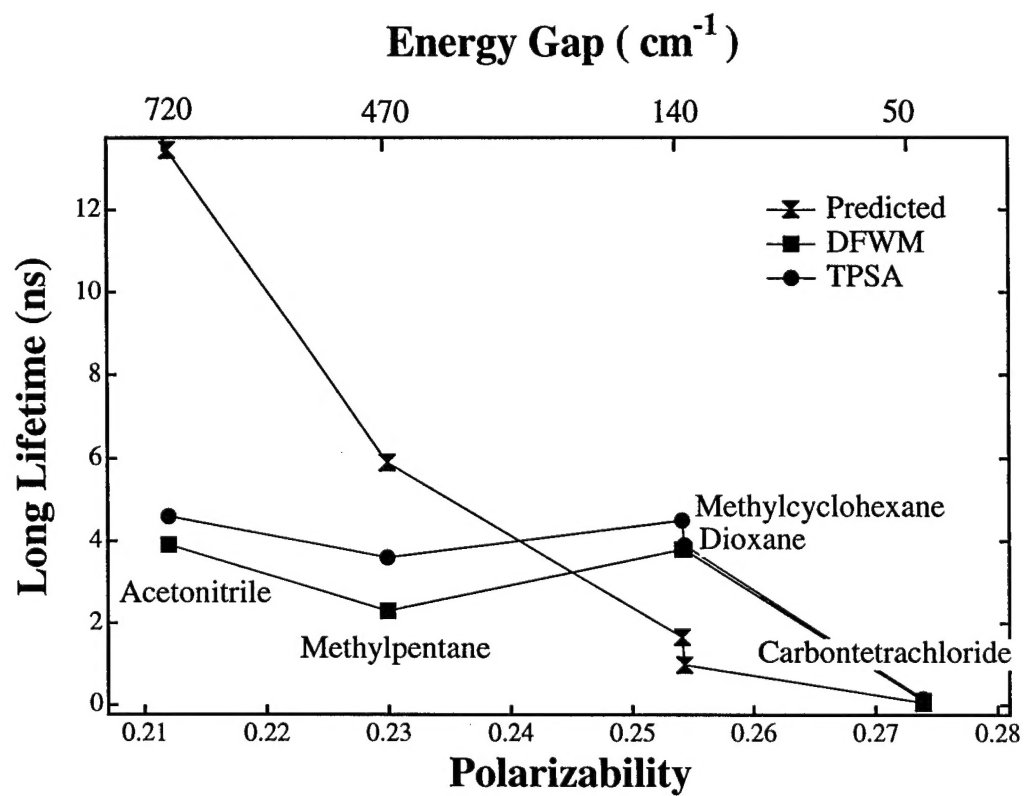
Figure 1.23 The lifetimes, τ_2, measured by DFWM experiments and by TPSA experiments compared to those predicted by the dynamical model.

Figure 1.23). The results show some differences between the experimental and the predicted lifetimes. These can be caused by the uncertainty in the values of energy gap as well as the lack of accurate values of k_2, which are estimated to be 35 times as large as k_1 [53].

5.0 Experimental Conclusion

The observed time evolution of the third order nonlinear optical susceptibility $\chi_{xyyx}^{(3)}(-\omega;\omega,\omega,-\omega)$ reveals that the dynamics of the enhanced nonlinear optical susceptibility $\chi_{xyyx}^{(3)}(-\omega;\omega,\omega,-\omega)$ of DPH can be accurately described by the population dynamics of a three level system. The results are also verified by separate transient pump-probe saturable absorption (TPSA) experiments that study the dynamics of the excited state populations. $\chi_{xyyx}^{(3)}(-\omega;\omega,\omega,-\omega)$ exhibits two-component exponential decay, with two characteristic lifetimes, which are strongly dependent on the solvent. For DPH in most solvents, energy gaps comparable to the thermal energy are also observed. The values of the third order nonlinear optical susceptibilities for the first two excited states of DPH are also determined.

Conclusion

Understanding the dynamics of the enhancement of the third order nonlinear optical susceptibility $\chi_{ijkl}^{(3)}(-\omega_4;\omega_1,\omega_2,\omega_3)$ is an important step toward the development of materials with higher nonlinear responses. We have shown, through the study of the time

evolution of $\chi^{(3)}_{xyyx}(-\omega;\omega,\omega,-\omega)$, that the dynamics of the enhancement of the third order nonlinear optical susceptibility exactly follows the population dynamics of a multilevel system.

The excited state enhancement of the third order nonlinear optical susceptibility $\chi^{(3)}_{ijkl}(-\omega_4;\omega_1,\omega_2,\omega_3)$ was theoretically predicted by many-electron interaction calculations of the molecular third order nonlinear optical susceptibility $\gamma_{ijkl}(-\omega_4;\omega_1,\omega_2,\omega_3)$ of conjugated linear chains when either the first or second π-electron excited state is occupied. The experimental observation of the enhancement of $\chi^{(3)}_{xyyx}(-\omega;\omega,\omega,-\omega)$ without any excited state absorption was made in nonresonant degenerate four wave mixing (DFWM) measurements at 1064 nm when the conjugated linear chain DPH solutions were optically pumped at 355 nm into the first one-photon allowed electronic excited state S_2 (1^1B_u).

This dissertation describes the dynamics of the excited state enhanced $\chi^{(3)}_{xyyx}(-\omega;\omega,\omega,-\omega)$, which exhibits two-component exponential decay with two characteristic lifetimes. These two lifetimes are also predicted by the dynamical model describing the population dynamics of the three level system. The short lifetime, in the picosecond timescale, corresponds to the time needed to reach thermal equilibrium between two excited states, S_1 (2^1A_g) and S_2 (1^1B_u). The long lifetime, in the nanosecond timescale, corresponds to the decay of both excited states, in thermal equilibrium, to the ground state S_0 (1^1A_g). The fact that the dynamical model is found to accurately describe the observed time-evolved third order nonlinear optical susceptibility $\chi^{(3)}_{xyyx}(-\omega;\omega,\omega,-\omega)$, confirms that the dynamics of $\chi^{(3)}_{xyyx}(-\omega;\omega,\omega,-\omega)$ follow that of the excited state populations. The results are also separately verified by transient pump-probe saturable

absorption (TPSA) experiments that study only the dynamics of the excited state populations.

From the analysis of the magnitude of the time evolved $\chi^{(3)}_{xyyx}(-\omega;\omega,\omega,-\omega)$, the values of the individual molecular isotropically third order nonlinear optical susceptibilities $\gamma^{S_n}(-\omega;\omega,\omega,-\omega)$ of DPH are calculated. Large $\gamma^{S_2}(-\omega;\omega,\omega,-\omega)$ of DPH in solvents used range from $42,000-60,900\times10^{-36}$ esu with a $\gamma^{S_1}(-\omega;\omega,\omega,-\omega)$ of $22,500\pm3,000\times10^{-36}$ esu, compared to the ground state $\gamma^{S_0}(-\omega;\omega,\omega,-\omega)$ which is less than 200×10^{-36} esu. In addition, energy gaps of 140 ± 50 cm^{-1} in dioxane and methylcyclohexane, 470 ± 70 cm^{-1} in methylpentane, and 720 ± 90 cm^{-1} in acetonitrile were also determined. There are still some differences between the predicted values of the two lifetimes and the observed values from both the DFWM and the TPSA experiments, which can be due to the uncertainty in the energy gap and the simplicity of the model, as well as the lack of accurate values for the fluorescence decay rates from the S_2 state to the ground states.

Future work on the dynamical model, new and more accurate methods of finding the energy gap values and decay rates, as well as time evolution experiments using shorter pulse widths, will provide more insight into the dynamical process.